THE CHEMISTRY AND ELECTROCHEMISTRY OF MAGNESIUM PRODUCTION

GEORGES J. KIPOUROS* AND DONALD R. SADOWAY

Department of Materials Science and Engineering
Massachusetts Institute of Technology
Cambridge, Massachusetts 02139

1. INTRODUCTION

A cubic kilometer of seawater contains approximately a million tonnes† of magnesium (1), more than has ever been produced in one year by all the magnesium plants in the world. Furthermore, seawater contains only 3.7% of the total magnesium present in the earth's crust (2). Clearly, magnesium resources are ubiquitous and virtually inexhaustible.

Due to its reactivity, magnesium is never found in nature in its free state but rather in compounds: as chloride in seawater (0.25-0.55%), in underground brines (up to 20%), and in salt deposits such as carnallite ($MgCl_2 \cdot KCl \cdot 6H_2O$), and as carbonates in the ores dolomite ($MgCO_3 \cdot CaCO_3$) and magnesite ($MgCO_3$). Less important are the surface minerals, kieserite ($MgSO_4 \cdot H_2O$), kainite ($MgSO_4 \cdot KCl \cdot 3H_2O$) and langbeinite ($2MgSO_4 \cdot K_2SO_4$).

Metallic magnesium is silvery-white. It belongs to the second group of the Periodic Table and has a valence of 2. There are three isotopes with mass numbers 24, 25, and 26 which occur naturally in the respective amounts 78.70%, 10.13%, and 11.17%. The electronic configuration in free atoms is (2)(8)(2). The chemistry of the element has been dealt with in monographs (1,3).

Magnesium melts at 651°C; its normal boiling point is 1120°C. The metal has a close-packed hexagonal crystal structure with a density of 1.74 g cm^{-3} at room temperature. It is this low density combined with favorable specific strength that makes magnesium attractive as a material.

---

* present address: General Motors Research Laboratories,
Electrochemistry Department, Warren, MI 48090.

† 1 tonne = 1 metric ton = 1000 kg.

In terms of production capacity, magnesium is the third most abundant structural metal: 4.5 times lighter than iron and 1.6 times lighter than aluminum, magnesium is by far the least dense of the three. The mechanical properties of magnesium castings make them competitive with aluminum castings. When hot worked, magnesium is the easiest to deep draw of the common metals and requires the least energy to machine. It has high damping capacity which is attributed to its high stiffness.

Table 1 gives the chemical requirements of the common grades of pure magnesium as specified by the standard set by the American Society for Testing and Materials, ASTM B 92 - 80 (Reapproved 1985) (4).

TABLE 1. Chemical requirements of pure magnesium.

	Composition, %				
	Grade 9980A	Grade 9980B	Grade 9990A	Grade 9995A	Grade 9998A
Aluminum, max	....	.....	0.003	0.01	0.004
Copper, max	0.02	0.02	.....	....	0.0005
Iron, max	....	....	0.04	0.003	0.002
Lead, max	0.01	0.01	....	....	0.001
Manganese, max	0.10	0.10	0.004	0.004	0.002
Nickel, max	0.001	0.005	0.001	0.001	0.0005
Silicon, max	....	....	0.005	0.005	0.003
Tin, max	0.01	0.01	....	....	....
Titanium, max	....	....	....	0.01	0.001
Other impurities each, max[A]	0.05	0.05	0.01[B]	0.005[B]	0.005[B]
Magnesium, by difference, min	99.80	99.80	99.90	99.95	99.98

[A] For specific applications, other minor impurities may be required to be controlled to limiting maxima by agreement between the purchaser and the seller.

[B] For nuclear applications, the cadmium and boron (high-capture cross-section elements) shall be specified as follows:

Cadmium, max, %	0.0001 or 0.00005
Boron, max, %	0.00007 or 0.00003

Further improvement in properties is achieved by the addition of alloying elements. Some of these are aluminum, manganese, silicon, zirconium, thorium, silver, rare earths, zinc, and lithium. Alloying changes not only the chemical properties of magnesium, e.g., corrosion resistance and pyrophoricity, but also the mechanical properties which depend on both the composition and the microstructure. Magnesium alloys can be fabricated by casting, rolling, forging, and extrusion.

Magnesium is used as a chemical reagent and as a material of construction.

The consumption of the metal can be broken down as follows (5): about 45% is used in aluminum alloys; another 35% is used for the manufacturing of chemicals, munitions, and fertilizers, in the desulfurization of steel, in metallothermic production of titanium, zirconium, beryllium, and uranium, and as sacrificial anodes for cathodic protection of other metals. Only about 20% is used in structural applications: it is here that the metal has its greatest potential.

There are two principal methods of producing magnesium metal: electrolysis of molten salts and metallothermic reduction. Both have a long history. Following the discovery of the metal in the form of an amalgam in 1808 by Sir Humphrey Davy, the isolation of free metallic magnesium was achieved for the first time in 1831 by Bussy (3) by heating magnesium chloride with potassium. Faraday, in 1833, was the first to obtain magnesium by electrolysis of fused magnesium chloride. Commercial activity based on the electrolysis of fused magnesium chloride began in Germany in the late 19th century. At the same time the reduction of alkaline earth oxides by aluminum was demonstrated by Mallet (6). Silicothermic reduction, the basis of the other present industrial practice, was first achieved in 1917 (6). Electrolysis of fused salts and silicothermic reduction account for 80% and 20%, respectively, of the current world production of magnesium.

Depending largely upon the magnesium resources available, two distinct processes have been advanced for each of the two reduction routes. The electrolytic methods are divided by cell feed into hydrous (Dow Chemical Process) and anhydrous (I. G. Farben - Norsk Hydro - VAMI*). Furthermore, different cell feeds result in different cell designs and operating practices. For example, because Soviet practice is to produce anhydrous feed from carnallite ($MgCl_2 \cdot KCl \cdot 6H_2O$), VAMI cell design differs from that of Norsk Hydro which uses brine as its raw material. Metallothermic reduction with silicon may be achieved either by externally supplied heat and collection of magnesium in the solid state (Pidgeon process) or by internally supplied electric heat and collection of magnesium in the liquid state (Magnetherm process). Non-electrolytic methods also include attempts to use other reductants such as carbon (carbothermic reduction), aluminum, or calcium carbide.

The extraction and processing of magnesium are described in textbooks (2,7-11), review articles (6), and chapters (1,12-14). The economics of

* Vsesoyuzny Alyuminievy i Magniyevy Institut (All-Union Aluminum and Magnesium Institute) Leningrad, U.S.S.R.

magnesium production have been analyzed (15-17) and the utilization of magnesium has been studied (18-20). Much of the patent literature is cited in the article by Lockwood, Ansel and Haddad (1). The paper by Schultz, Neelameggham, Agarwal and Hammersley (5) is useful for its historical consumption and production data as well as for its forecasting of potential growth areas in the use of magnesium.

Despite the availability of numerous references, much less is revealed in the open literature about magnesium extraction than about steelmaking or aluminum production. This is in some measure due to the fact that these other structural metals are produced in far greater quantities than magnesium, and thus the research efforts in steel and aluminum have been proportionately much more substantial. In particular, very little is written about the scientific fundamentals of the various magnesium extraction processes. Thus, it is the purpose of this article to interpret the present practice of magnesium production in the light of the relevant chemistry and electrochemistry.

2. ELECTROLYTIC METHODS OF MAGNESIUM PRODUCTION

With an electronegative standard potential of -2.4 V, magnesium lies near the end of the electromotive series; thus its electrolytic recovery from aqueous media is very difficult and impractical. Furthermore, its high affinity for oxygen, as demonstrated by the extreme stability of magnesium oxide ($\Delta_f G^\circ$ = -493 kJ per mole MgO at 1000 K (21)), effectively dictates that any nonaqueous electrolyte used for the recovery of magnesium metal be free of oxygen. Thus, all electrolytic magnesium processes employ molten halide electrolytes. Magnesium is fed into the cell in the form of magnesium chloride, its preparation being the first step of the process. The extent of dehydration of the cell feed is the major difference between the two industrial electrolytic practices.

2.1 Cell Feed Preparation

Preparation of magnesium chloride involves the chlorination of magnesium oxide produced either by calcination of magnesite or by precipitation of magnesium hydroxide with the aid of dolomite or some other suitable form of alkalinity. Figure 1 depicts the steps for cell feed preparation for both electrolytic processes, hydrous (Dow Chemical) and anhydrous (I. G. Farben - Norsk Hydro - VAMI). Both methods involve the common step of precipitating magnesium hydroxide followed either by the production of a 35% magnesium chloride brine (Dow Chemical) or by calcination to magnesium oxide and

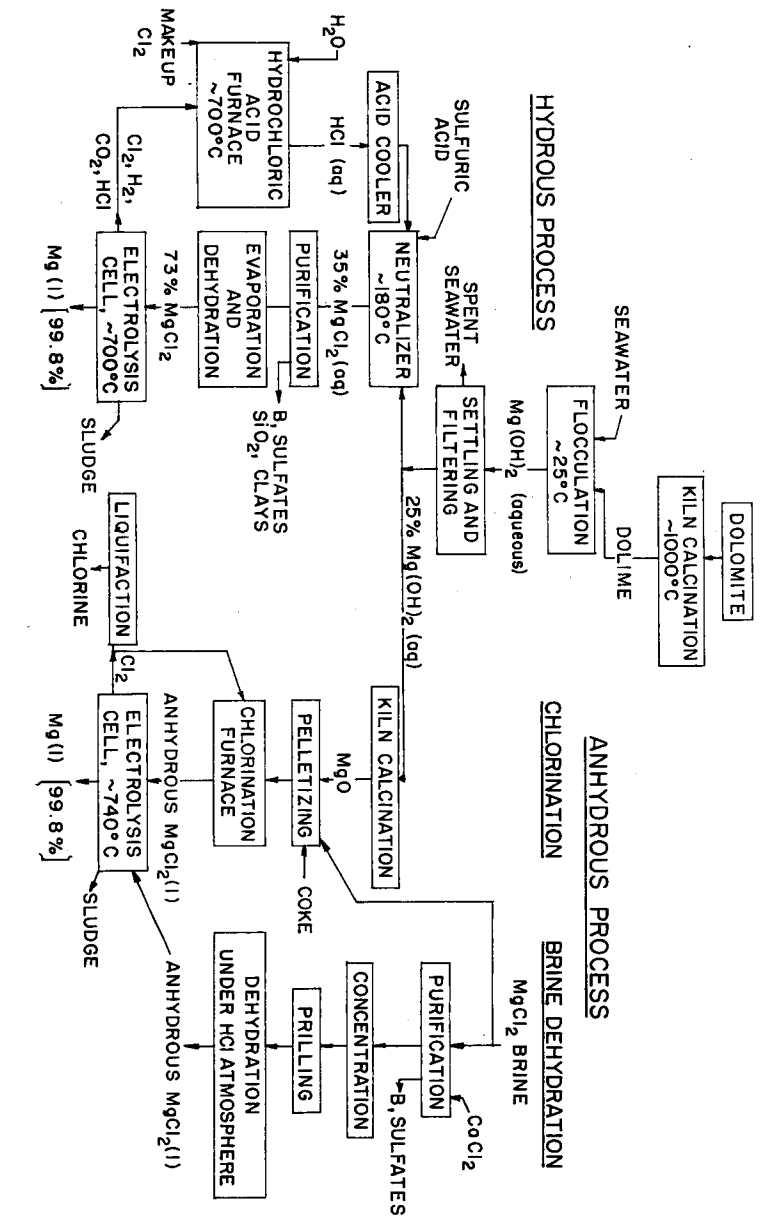

Figure 1. Flowsheet for the preparation of cell feed (schematic).

subsequent chlorination yielding anhydrous magnesium chloride (I. G. Farben - Norsk Hydro - VAMI). A new method of producing anhydrous magnesium chloride has been described (22) which is based entirely on the evaporation of magnesium chloride brine. First, impurities such as boron and sulfate, which are detrimental to electrolysis, are removed, and the brine is concentrated to about 50%. The final step is a careful extraction of water from the hydrated solid, which is in a prilled form, in a hydrogen chloride atmosphere. Prilling is the term for spray solidifying molten salts to form small spheroids.

Although it is not the only harmful impurity present, water is an unwanted component of the cell feed for many reasons: (a) it reacts with $MgCl_2$ at the temperature of electrolysis to form hydrogen chloride gas which both causes corrosion in the cell and renders the chlorine produced at the anode unmarketable; (b) it wears the anodes, causing dimensional instability and shortening their lives and (c) it interferes with the cathodic reaction by preventing the coalescence of magnesium droplets. However, magnesium chloride is very hygroscopic. Furthermore, as shown in Figure 2, water can become chemically bound to form a series of hydrate compounds with magnesium chloride (23,24). Actually, Figure 2, which is the water-rich half of the $MgCl_2$-H_2O phase diagram, corrects several errors that have become entrenched in the magnesium literature over the years and displays the data in a metallurgical format. It is evident that, except for the dodecahydrate, the hydrates all melt incongruently. Earlier diagrams failed to show this; instead, in many cases the respective liquidus lines were labeled as the hydrate compound. Finally, the compound $MgCl_2 \cdot 12H_2O$ forms a simple eutectic with water, a fact not evident in earlier diagrams.

2.1.1 Dehydration of magnesium chloride

According to the phase diagram of Figure 2, at room temperature the most fully hydrated form of magnesium chloride is the hexahydrate, $MgCl_2 \cdot 6H_2O$. Its dehydration proceeds by the following reaction:

$$MgCl_2 \cdot 6H_2O = MgCl_2 \cdot 4H_2O + 2H_2O(g) \qquad (1)$$

over the temperature range 298-390 K, where the hexahydrate is stable. The equilibrium constant of reaction (1), K_1, may be written as

$$K_1 = \ln P^2_{H_2O} \qquad (2)$$

provided that it is assumed that the hydrates are mutually insoluble. The

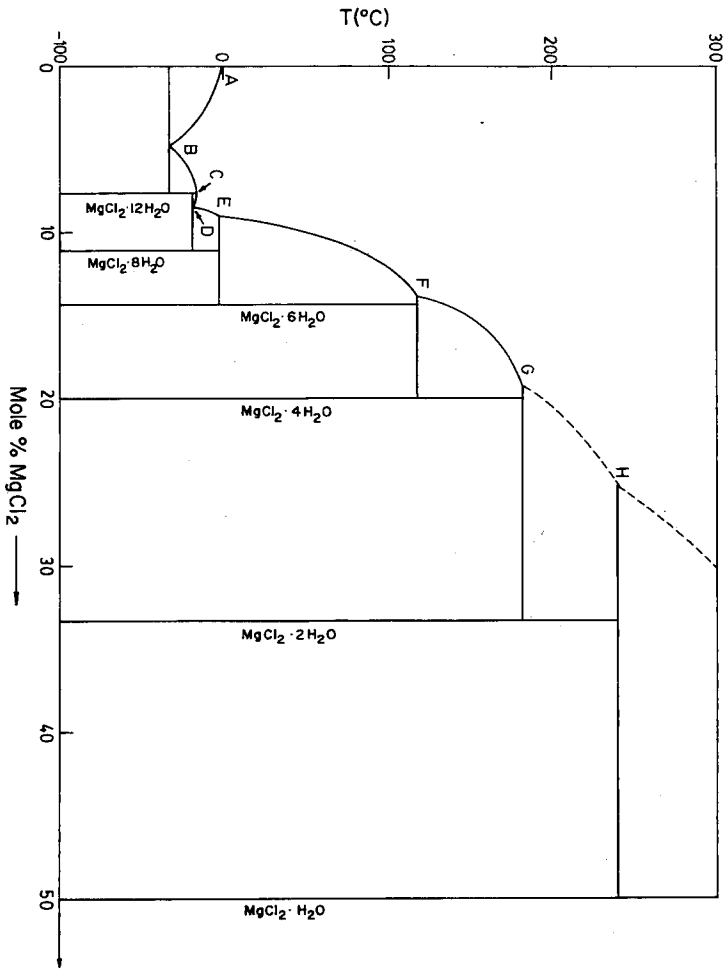

Figure 2. Phase diagram of the system $MgCl_2$-H_2O (schematic).

LEGEND

	%$MgCl_2$	(°C)
A	0.	0.
B	4.9	-33.6
C	7.7	-16.4
D	8.0	-16.8
E	9.0	-3.4
F	13.9	116.7
G	19.2	181.5
H		240.

temperature dependence of the vapor pressure of water can be calculated from the free energy of reaction:

$$\Delta G_1^\circ = -RT\ln K_1 = -2RT\ln P_{H_2O} \quad (3)$$

to give the following relationship (25,26):

$$\log P_{H_2O} = 6.335 - 0.608\times10^{-3}T + 0.421\log T - 3{,}039T^{-1} \quad (4)$$

where T is in Kelvin and P is in torr.

Figure 3 shows this graphically as a plot of log P_{H_2O} versus T. The broken line, FG, represents the estimated water vapor pressure in equilibrium with the solid tetrahydrate and "molten hexahydrate," or more precisely, the melt at the respective liquidus composition. The points F, G, and H represent the same conditions in Figure 3 as they do in the phase diagram of Figure 2.

The dehydration of $MgCl_2\cdot4H_2O$ occurs by conversion to the dihydrate by the reaction

$$MgCl_2\cdot4H_2O = MgCl_2\cdot2H_2O + 2H_2O(g) \quad (5)$$

for which the equilibrium constant is

$$K_5 = P^2_{H_2O} \quad (6)$$

Following the procedure described above, the temperature dependence of the water vapor pressure is found to be

$$\log P_{H_2O} = 8.248 - 0.608\times10^{-3}T + 0.075\log T - 3{,}605T^{-1} \quad (7)$$

where T is in Kelvin and P is in torr. Equation (7) is also plotted in Figure 3 over the temperature range where the tetrahydrate is stable. The broken line GH represents the estimated water vapor pressure in equilibrium with the solid dihydrate and "molten tetrahydrate."

Dehydration of the dihydrate by conversion to the monohydrate occurs by the reaction

$$MgCl_2\cdot2H_2O = MgCl_2\cdot H_2O + H_2O(g) \quad (8)$$

for which the equilibrium constant is

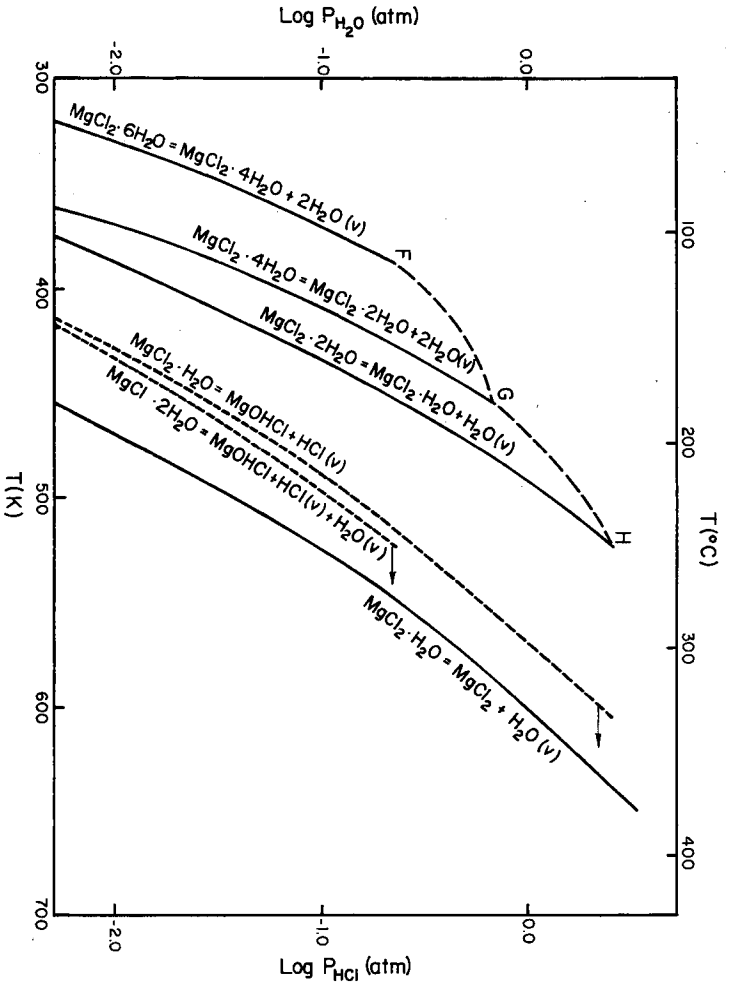

Figure 3. Vapor pressures of H_2O or HCl over the magnesium chloride hydrates.

$$K_8 = P_{H_2O} \quad (9)$$

The temperature dependence of the equilibrium water vapor pressure over the dihydrate is

$$\log P_{H_2O} = 9.242 - 0.608\times10^{-3}T - 0.428\log T - 3.833T^{-1} \quad (10)$$

where T is in Kelvin and P is in torr. Equation (10) is plotted in Figure 3 over the temperature range where the dihydrate is stable.

It should be noted that dehydration of the dihydrate can also proceed by hydrolysis:

$$MgCl_2\cdot 2H_2O = MgOHCl + HCl(g) + H_2O(g) \quad (11)$$

The equilibrium constant of this reaction is

$$K_{11} = P_{HCl}\cdot P_{H_2O} \quad (12)$$

and its temperature dependence may be expressed as

$$\log P_{HCl}\cdot P_{H_2O} = 18.866 - 1.060\times10^{-3}T - 1.259\log T - 7,895T^{-1} \quad (13)$$

Reaction (11) is inhibited by the greater vapor pressure of water generated by reaction (8) which occurs simultaneously. To deter hydrolysis entirely, a minimum partial pressure of HCl must be applied. This minimum pressure can be calculated from equation (13), when values of P_{H_2O} calculated from equation (10) are used. The results are plotted in Figure 3.

The final stage in dehydrating magnesium chloride is to remove the last water of crystallization from the monohydrate by the reaction

$$MgCl_2\cdot H_2O = MgCl_2 + H_2O(g) \quad (14)$$

for which the equilibrium constant is

$$K_{14} = P_{H_2O} \quad (15)$$

the temperature dependence of the water vapor pressure is

$$\log P_{H_2O} = 9.049 - 0.608\times10^{-3}T - 0.452\log T - 4.471T^{-1} \quad (16)$$

Equation (16) is plotted in Figure 3, which also shows the partial pressure of HCl for the corresponding hydrolysis reaction,

$$MgCl_2\cdot H_2O = MgOHCl + HCl(g) \quad (17)$$

The equilibrium vapor pressure of HCl generated by reaction (17) can be calculated as described above:

$$\log P_{HCl} = 9.633 - 0.452\times10^{-3}T - 0.830\log T - 4,042T^{-1} \quad (18)$$

Reactions (14) and (17) may be combined to express the hydrolysis of $MgCl_2$ as

$$MgCl_2 + H_2O(g) = MgOHCl + HCl(g) \quad (19)$$

which allows a calculation of the minimum ratio of P_{HCl}/P_{H_2O} to avert hydrolysis. As shown in Figure 3, the vapor pressure of HCl is considerably higher than the vapor pressure of H_2O. This suggests that if precautions are not taken, the hydrolysis reaction (17) will proceed in preference to the dehydration reaction (14). Alternatively, hydrolysis can be averted when the applied partial pressure of HCl exceeds that shown in Figure 3 for reaction (17).

A final note on the dehydration of magnesium chloride concerns the stability of the oxychloride, MgOHCl, which may decompose according to the reaction

$$MgOHCl = MgO + HCl(g) \quad (20)$$

for which the equilibrium pressure of HCl is

$$\log P_{HCl} = 1.309 - 0.228\times10^{5}T^{-2} - 1.359\times10^{-3}T + 2.094\ \log T - 5,181T^{-1} \quad (21)$$

The decomposition temperature of MgOHCl, i.e., the temperature at which the pressure of HCl reaches 1 atmosphere, is calculated from equation (21) to be 828 K. Above this temperature the oxychloride formed during dehydration will be converted entirely to MgO according to reaction (20).

In the light of the above, the commercial practice for magnesium chloride can

be explained. Under equilibrium conditions the dehydration of magnesium chloride hexahydrate to dihydrate presents no particular problem. The dehydration may be conducted by passing hot dry air or heated combustion products over the reactant and will follow reactions (1) and (5) as shown in Figure 3. To avoid hydrolysis, the evaporation may be conducted by spraying into a stream of hot HCl gas. Dehydration by heating beyond the dihydrate requires special precautions. Simple heating without an HCl atmosphere will follow the hydrolysis curves as shown in Figure 3 and will eventually lead to the formation of MgOHCl. However, careful dehydration in a stream of dry HCl gas will suppress the hydrolysis reactions (11) and (17), and the dehydration will proceed according to reactions (8) and (14) as indicated in Figure 3.

It should be noted that Figure 3 presents data derived on the basis of purely thermodynamic considerations, i.e., under equilibrium conditions. In industrial practice, kinetic factors which do not appear to have been extensively studied in this system are exploited. Indeed, spray drying under optimum conditions can produce material with 1% H_2O and 1% MgO, although normal practice gives 2 - 5% H_2O and 2 - 5% MgO.

Thus, there is no clear choice for the extent of dehydration of magnesium chloride. Complete dehydration to produce anhydrous cell feed is energy intensive but allows for a more efficient electrolysis to produce not only magnesium metal but also marketable chlorine. Partial dehydration to produce hydrous cell feed requires less energy than complete dehydration; however, electrolysis of hydrous $MgCl_2$ consumes anode carbon and, without further processing, does not produce marketable chlorine. Local economics determine the approach, and both approaches are currently in use. Commercial equipment is described in the literature (1,2,13,22). To reduce the energy requirements of dehydration, solar drying is employed in several processing sequences (27,28).

To avoid some of the problems presented by the dehydration of hydrated magnesium chloride, other processes for cell feed preparation have been investigated. These include dehydration of double salts and chlorination of magnesium oxide and are discussed below.

2.1.2 Dehydration of double salts

Magnesium chloride and potassium chloride form a hydrated double salt called carnallite, $KCl \cdot MgCl_2 \cdot 6H_2O$. Since KCl is also a major component of the electrolyte, one option in cell feed preparation is to produce anhydrous $KCl \cdot MgCl_2$ directly from carnallite.

The dehydration of carnallite proceeds according to the reactions

$$KCl \cdot MgCl_2 \cdot 6H_2O = KCl \cdot MgCl_2 \cdot 2H_2O + 4H_2O(g) \quad (22)$$

and

$$KCl \cdot MgCl_2 \cdot 2H_2O = KCl \cdot MgCl_2 + 2H_2O(g) \quad (23)$$

accompanied to a certain extent by hydrolysis according to reaction (11). Although it appears that dehydration of carnallite is similar to that of magnesium chloride, there is a significant difference between the two. Any oxychloride generated during the dehydration of carnallite forms a solid solution with it. Upon melting, the oxychloride dissociates according to

$$MgOHCl = MgOH^+ + Cl^- \quad (24)$$

thereby generating cationic impurities which can interfere with the electrochemical reduction of magnesium in the electrolytic cell. To prevent hydrolysis a blanket of dry hydrogen chloride gas should be present. Thus, the process becomes as complicated as the dehydration of magnesium chloride and appears to offer no advantages over the latter. Furthermore, long term cell feeding with dehydrated carnallite eventually requires either that pure $MgCl_2$ make-up be added or that supporting electrolyte be withdrawn to keep its composition within limits.

Using thermogravimetry, differential thermal analysis, and thermooptical analysis, Emons et al. (29) characterized the melting and decomposition behavior of carnallite. They found that the final product of thermal decomposition is not pure $KCl \cdot MgCl_2$ as written in equation (23) but rather $KMgCl_x(OH)_y$, where $2.84 < x < 2.90$ and $0.10 < y < 0.16$. The effect of changes in the partial pressures of H_2O and HCl was to shift the decomposition temperatures. In part, the inability to produce pure anhydrous $KCl \cdot MgCl_2$ is explained by the existence of a stable weakly basic monohydrate in the temperature range, $235° < T < 290°$ C (30).

Another double salt is ammonium carnallite, $NH_4Cl \cdot MgCl_2 \cdot 6H_2O$. It is claimed that the ammonium chloride protects the magnesium chloride from hydrolysis (31). Dehydration occurs in the following steps:

$$NH_4Cl \cdot MgCl_2 \cdot 6H_2O \xrightarrow{373\ K} NH_4Cl \cdot MgCl_2 \cdot 4H_2O + 2H_2O\ (g) \quad (25)$$

$$NH_4Cl \cdot MgCl_2 \cdot 4H_2O \xrightarrow{413\ K} NH_4Cl \cdot MgCl_2 \cdot 2H_2O + 2H_2O\ (g) \quad (26)$$

$$NH_4Cl \cdot MgCl_2 \cdot 2H_2O \xrightarrow{433\ K} NH_4Cl \cdot MgCl_2 + 2H_2O\ (g) \quad (27)$$

$$NH_4Cl \cdot MgCl_2 \xrightarrow{509\ K} NH_4Cl + MgCl_2 \quad (28)$$

Heating ammonium carnallite to 450 K will result in dehydration according to reactions (25-27). In a second step reaction (28) is carried out by maintaining a temperature of 573 K. The last step should be conducted upon complete removal of the water of crystallization, otherwise hydrolysis will occur via reaction (19). The patent literature (1) describes several variations of this method of dehydration. Recent studies describe the dehydration of ammonium chloride in an NH_3 atmosphere (32) or in the presence of an organic phase (33).

Although dehydration of double salts has its merits, there has been little commercial utilization of the method. It seems that the higher energy consumption offsets the advantages. Carnallite dehydration has been used on an industrial scale in the USSR (1). Ammonium carnallite dehydration has been practiced on a laboratory scale by the authors of the present article. The product anhydrous $MgCl_2$ was then sublimed in an inert atmosphere containing $SOCl_2$ to give a highly purified material for spectral studies (34).

2.1.3 Chlorination of magnesium oxide

Difficulties in the dehydration of $MgCl_2 \cdot 6H_2O$ led to the development of processes for the direct chlorination of magnesium oxide. As shown in Figure 1, magnesium oxide is produced by calcination (~1000°C) of either magnesite or $Mg(OH)_2$ precipitated by mixing seawater with dolime.

The chlorination of magnesium oxide may be represented by the reaction

$$MgO + Cl_2 = MgCl_2(s \text{ or } \ell) + \tfrac{1}{2}O_2 \quad (29)$$

where $MgCl_2$ is solid below 987 K and molten above this temperature. The equilibrium constants may be written as

$$K_{29} = P_{O_2}^{\frac{1}{2}}/P_{Cl_2} \quad (30)$$

This assumes that MgO and $MgCl_2$ are mutually insoluble. The standard enthalpy and free energy of reaction calculated from available thermodynamic data are given by equations (31) and (32):

$$\Delta H^\circ_{29} = -2{,}247 + 6.165T - 0.369\times10^{-3}T^2 - 2.087\times10^{5}T^{-1} \quad (31)$$

$$\Delta G^\circ_{29} = -2{,}247 + 47.345T - 6.165T\ln T + 0.369\times10^{-3}T^2 - 1.044\times10^{5}T^{-1} \quad (32)$$

in calories. At 1300 K, which is the temperature at which industrial chlorination reactors operate, the oxygen content of the gas should be kept below 1.4 mole percent at 1 atmosphere total pressure. Failure to achieve this will result in oxidation of $MgCl_2$, i.e. reaction (29) proceeds to the left. In industrial practice, to perform the chlorination at an acceptable rate, the pressure of oxygen will increase above the equilibrium value. Thus the need will arise to bind the evolved oxygen by a suitable reducing agent such as carbon.

Carbochlorination occurs by the reaction

$$MgO + Cl_2 + C = MgCl_2(\ell) + CO \quad (33)$$

with a standard enthalpy of reaction

$$\Delta H^\circ_{33} = -27{,}680 + 5.45T - 0.79\times10^{-3}T^2 - 4.177\times10^{5}T^{-1} \quad (34)$$

At 1300 K this gives $\Delta H^\circ = -22$ kcal: the reaction is highly exothermic and largely self-sustaining once begun.

The standard free energy of carbochlorination is given as

$$\Delta G^\circ_{33} = 27{,}680 - 5.45T\ln T + 0.79\times10^{-3}T^2 - 2.088\times10^{5}T^{-1} + 19.66T \quad (35)$$

At 1300 K, this gives $\Delta G^\circ = -52$ kcal. The reaction products are very stable. Thus, when a stream of chlorine gas passes through a mixture of MgO and C maintained at a constant temperature of 1300 K the gas phase will consist almost entirely of CO provided that equilibrium is achieved. On the other hand, since most industrial chlorination reactors have been designed to consume a minimum amount of reagent (carbon) and do not operate isothermally, the gas phase tends to be a mixture of CO, CO_2, Cl_2 and volatile chlorides.

Carbon monoxide itself, however, is also a reducing agent initiating a strongly exothermic reaction,

$$MgO + Cl_2 + CO = MgCl_2(\ell) + CO_2 \quad (36)$$

with a standard enthalpy given by

$$\Delta H^\circ_{36} = -70{,}720 + 6.70T - 0.11\times10^{-3}T^2 - 0.132\times10^{5}T^{-1} \quad (37)$$

and a standard free energy of

$$\Delta G^\circ_{36} = -70{,}720 - 6.70T\ln T + 0.11\times10^{-3}T^2 - 0.066\times10^{5}T^{-1} + 72.91T \quad (38)$$

The equilibrium composition of the gas phase of the chlorinator can be calculated from equations (33) and (36). At a total pressure of 1 atmosphere the gas composition is given by simultaneous solution of the following equations:

$$P_{CO}/P_{Cl_2} = \exp -(\Delta G^\circ_{33}/RT) \quad (39)$$

$$P_{CO_2}/(P_{Cl_2}\cdot P_{CO}) = \exp -(\Delta G^\circ_{36}/RT) \quad (40)$$

$$P_{CO} + P_{Cl_2} + P_{CO_2} = 1. \quad (41)$$

At 987 K, the melting point of $MgCl_2$, this gives $P_{Cl_2} = 8 \times 10^{-11}$ atm, $P_{CO} = 0.67$ atm, and $P_{CO_2} = 0.33$ atm, i.e., the gas contains practically no chlorine while the equilibrium content of CO_2 is about 33%. Similar calculations for a temperature of 1300 K yield $P_{Cl_2} = 2 \times 10^{-9}$ atm, $P_{CO} = 0.995$ atm, and $P_{CO_2} = 0.005$ atm, which indicates that reaction (36) is hardly utilized at all. Proper control of the temperature of the chlorination furnace is therefore essential for its successful operation.

In a recent patent (35) the carbochlorination of magnesium carbonate (instead of magnesium oxide) by chlorine and carbon monoxide gases in a packed bed reactor to produce anhydrous molten magnesium chloride is described. The reaction is

$$MgCO_3(s) + CO + Cl_2 = MgCl_2(\ell) + 2CO_2 \quad (42)$$

Carbon dioxide is removed from the top of the reactor; anhydrous molten magnesium chloride is withdrawn below the packed bed. The energy requirements of this process are low, and the kinetics are favorable. In the 1920's

Goldschmidt (23) had proposed a reaction between $MgCO_3$ and $COCl_2$.

A detailed description of chlorination technology as it applies to MgO in general has been given elsewhere (2,13). The magnesium oxide is mixed with carbon and magnesium chloride which acts as a binder. This mixture is formed into pellets which are dried and fed into the top of an electrically heated shaft furnace while chlorine enters at the bottom. In a continuous operation molten magnesium chloride is tapped periodically into crucibles and fed to the electrolysis cells.

Recently the chlorination process has become the subject of re-examination for two main reasons. First, under certain conditions environmentally unacceptable polychlorinated hydrocarbons may be produced (13,22) and secondly, the chlorination furnaces are not easy to control (22). For improved efficiency it is necessary to optimize the charge with respect to particle size distribution, particle porosity, activity of the reducing agent, i.e. grade of carbon, as well as with respect to the concentrations of certain impurities.

2.1.4 Removal of impurities

Impurities in the electrolyte have several sources. Some are introduced into the cell as part of the feed. Others are products of reaction between the electrolyte and cell components, e.g., electrodes, cell walls, and cell products. Discussion of the effect of impurities on the electrolytic processes will be deferred to a later section. The removal of impurities normally introduced along with the cell feed will be discussed in this section.

Sources of $MgCl_2$ can also contain oxides and sulfates, as well as boron. Table 2 shows the maximum permissible levels of commonly occurring impurities. These should be viewed in the context of Table 1 which specifies the allowable impurities in magnesium metal.

When cell feed is produced by dehydration of hydrated magnesium chloride concentrated from seawater or brines, sulfates are removed as calcium sulfate. It was found (2) that the solubility of $CaSO_4$ decreases as $MgCl_2$ content increases. For a brine containing 35% $MgCl_2$ the solubility of $CaSO_4$ is 1.37 g/l. A similar trend has also been observed for $MgSO_4$. At this stage of brine concentration the sulfates are precipitated by the addition of $CaCl_2$ (22). This treatment also results in precipitation of other solids, such as clays and silica. In exceptional cases $BaCl_2$ may be added to remove the last traces of sulfate. Following this, boron is removed by ion exchange (13) or solvent extraction (10). In the seawater process the excess calcium precipitating along with magnesium with sulfuric acid after $Mg(OH)_2$ has been dissolved in HCl. The

TABLE 2. Maximum permissible levels of impurities in cell feed.

B	0.001%
MgO	0.2%
SO_4	0.05%
Fe	0.005%
C*	0.2%
H_2O*	0.1%
Ti**	0.005%
Mn**	0.1%

* for anhydrous feed
** for $MgCl_2$ recycled from Ti, Zr plants

residual sulfate is then removed by the addition of small amounts of barium carbonate or barium chloride.

When cell feed is prepared by carbochlorination of magnesium oxide, impurities are removed by different reactions. For example, the other oxides are also carbochlorinated by reactions such as

$$CaO + C + Cl_2 = CaCl_2 + CO \quad (43)$$

$$2Fe_2O_3 + 3C + 6Cl_2 = 4FeCl_3 + 3CO_2 \quad (44)$$

$$SiO_2 + 2C + 2Cl_2 = SiCl_4 + 2CO \quad (45)$$

$$2Al_2O_3 + 3C + 6Cl_2 = 4AlCl_3 + 3CO_2 \quad (46)$$

These reactions waste chlorine and carbon. Furthermore, not all the above reactions go to completion, and the remaining oxides, particularly SiO_2, MgO, and Al_2O_3, form a slag the removal of which complicates the operation.

Sulfates are also chlorinated according to the following reactions:

$$MgSO_4 + C + Cl_2 = MgCl_2 + SO_2 + CO_2 \quad (47)$$

$$CaSO_4 + C + Cl_2 = CaCl_2 + SO_2 + CO_2 \quad (48)$$

Finally, up to 50% of the moisture present can evaporate upon introduction into the furnace, while the rest is chlorinated according to the reactions

$$2H_2O + 2Cl_2 + C = 4HCl + CO_2 \quad (49)$$

$$H_2O + Cl_2 + C = 2HCl + CO \quad (50)$$

Reactions (49) and (50) are of importance not only in the chlorination process but also during electrolysis where the necessary carbon is supplied by the anode, which is consumed as a consequence. The final product of the chlorination process contains also some suspended solid particles of MgO and carbon. While the presence of carbon in the electrolyte can be considered beneficial from the standpoint of reducing anode consumption, there is an attendant rise in the electrical conductivity of the bath as a result. This will be seen in Section 2.2.2 to be detrimental to cell performance.

2.2 The Electrolyte

2.2.1 Decomposition potentials

The electrolysis cell performs the decomposition of molten magnesium chloride to produce liquid magnesium and chlorine gas by the reaction

$$MgCl_2(\ell) = Mg(\ell) + Cl_2(g) \quad (51)$$

From available thermodynamic data the standard free energy of reaction (51) is

$$\Delta G^\circ_{51} = 148{,}620 + 6.422T\ln T - 0.14\times10^{-3}T^2 - 77.47T \quad (52)$$

The standard reversible decomposition potential, E°, for reaction (51) is given by

$$\Delta G^\circ_{43} = -nFE^\circ \quad (53)$$

where n is the number of electrons taking part in the reaction, in this instance 2, and F is the Faraday, 23,061 calories per volt-equivalent. Substitution of (52) into (53) gives the temperature dependence of the standard reversible potential:

$$E^\circ_{MgCl_2} = -3.222 + 1.679\times10^{-3}T - 1.392\times10^{-4}T\ln T + 3.035\times10^{-9}T^2 \quad (54)$$

Equation (54) indicates that the standard reversible decomposition potential of magnesium chloride is a function only of temperature. Theoretically, it

would be possible to recover magnesium metal by electrolysis of pure magnesium chloride; however, this is impractical due to its high melting point and volatility and low electrical conductivity. Furthermore, the solubility of elemental magnesium in pure magnesium chloride is high enough to cause a significant decrease in current efficiency. In contrast, elemental magnesium is far less soluble in multicomponent melts (2).

To improve the above mentioned physicochemical properties, magnesium chloride is dissolved in a so-called 'supporting electrolyte' which consists of other chlorides. The decomposition potential of magnesium chloride in this solution can be calculated by combining equation (54) with the thermodynamic relations

$$\bar{\Delta G}_{MgCl_2} = -nFE \qquad (55)$$

where $\bar{\Delta G}_{MgCl_2}$ is the partial molar free energy of mixing of $MgCl_2$ in the melt and

$$\bar{\Delta G}_{MgCl_2} = RT \ln a_{MgCl_2} = \mu_{MgCl_2} - \mu^{\circ}_{MgCl_2} \qquad (56)$$

where a_{MgCl_2} is the chemical activity of $MgCl_2$ in the melt expressed with respect to a standard state of pure molten $MgCl_2$ at the same temperature, μ_{MgCl_2} is the chemical potential of $MgCl_2$ in the melt, and $\mu^{\circ}_{MgCl_2}$ is the chemical potential of pure molten $MgCl_2$ at the same temperature.

The result of combining equations (54), (55), and (56) is the Nernst equation:

$$E_{MgCl_2} = E^{\circ}_{MgCl_2} - (RT/2F)\ln a_{MgCl_2} \qquad (57)$$

Chemical activity can be expressed as the product of the activity coefficient, γ, and the concentration, typically expressed as mole fraction, X. Thus, equation (57) can be rewritten as

$$E_{MgCl_2} = E^{\circ}_{MgCl_2} - (RT/2F)\ln \gamma_{MgCl_2} - (RT/2F)\ln X_{MgCl_2} \qquad (58)$$

The isothermal variation in decomposition potential of magnesium chloride in a molten solution of KCl-NaCl at 973 K is shown in Figure 4, which has been drawn from data reported in the literature (36). E° is -2.517 V for pure molten

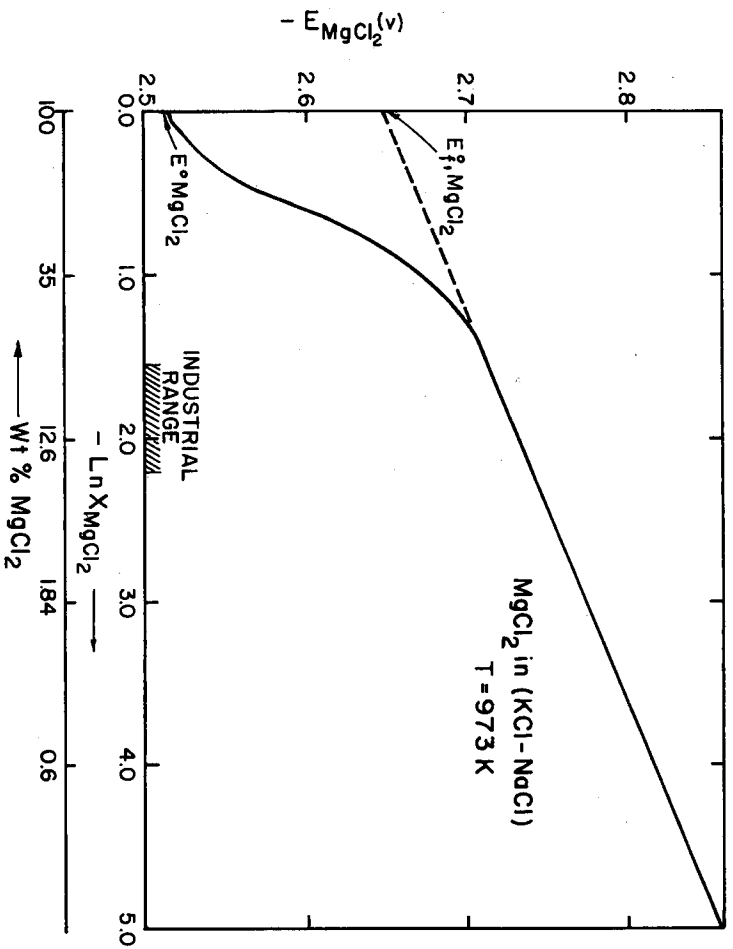

Figure 4. Variation of the reversible decomposition potential of $MgCl_2$ in KCl-NaCl as a function of concentration.

$MgCl_2$ at this temperature. As the concentration of $MgCl_2$ in the solution decreases, E decreases, i.e., becomes more negative. At high dilution $MgCl_2$ obeys Henry's law, and thus γ_{MgCl_2} is no longer a function of composition. Equation (58) shows that in the Henrian regime E varies linearly with $\ln X_{MgCl_2}$. The line has a "2-electron slope," i.e., -RT/2F. The extrapolation of this Henrian line to pure $MgCl_2$ gives a value of -2.624 V for the apparent standard decomposition potential as defined by Flengas (37).

The decomposition potentials of the other components of the electrolyte are also calculated by the analogous Nernst equations,

$$E_i = E_i^\circ - (RT/nF)\ln \gamma_i - (RT/nF)\ln X_i \qquad (59)$$

where E_i° is the standard decomposition potential of pure molten component i at the same temperature, and n is the number of electrons taking part in the reaction. Equation (59) limits the choice of components to those with decomposition potentials more negative than that of magnesium chloride. To give some indication of relative reducibility, Table 3 gives the standard

TABLE 3. Decomposition potentials of fused salts.

Metal Chloride	-E° (V) Temperature (K)		
	873	973	1073
$MgCl_2$	2.602	2.531	2.460
KCl	3.658	3.549	3.441
NaCl	3.424	3.332	3.240
$CaCl_2$	3.462	3.392	3.323
$BaCl_2$	3.728	3.648	3.568
LiCl	3.571	3.514	3.457
$MnCl_2$	1.902	1.854	1.807
$FeCl_2$	1.207	1.163	1.118
$FeCl_3$	-	0.780	-
$TiCl_2$	1.885	1.825	-
$TiCl_3$	-	1.817	-

decomposition potentials of a number of salts (37,38). While proper comparison must be based on the decomposition potentials calculated by equation (59), at a temperature of 1000 K the change from standard potential is only 198 mV for a monovalent cation at an activity of 0.1.

Also given in Table 3 are the decomposition potentials of some of the compounds that were included in Table 2 as impurities. Since these compounds, namely $MnCl_2$, $FeCl_3$, and $TiCl_4$, have standard decomposition potentials substantially higher, i.e. less negative, than that of magnesium chloride, they will tend to decompose in preference to the latter. To prevent electrolysis of contaminants their concentrations are maintained below the limits set in Table 2. Some of these reactive-metal chlorides are reduced by displacement reactions with elemental magnesium and collect in the cell sludge; others are electrolytically reduced and appear as impurities in the magnesium metal product.

For economic reasons the composition of the electrolyte depends to a great extent on the resources available. The following are reported to be industrial electrolytes (13). Concentrations are expressed in weight percent.

$MgCl_2$ dihydrate from seawater or brine sources	60% NaCl; 25% $MgCl_2$; 15% $CaCl_2$
$MgCl_2$ from brine	50% KCl; 35% NaCl; 15% $MgCl_2$; 3% $CaCl_2$ or a five component electrolyte containing Li, Na, K, Mg and Ca chlorides
$MgCl_2$ from seawater	40% $CaCl_2$; 30-40% NaCl; 5-20% KCl; 10-15% $MgCl_2$

Some barium chloride may also be present in the electrolyte depending on brine processing.

2.2.2 Physicochemical properties

The composition of the electrolyte is chosen not only on the basis of electrochemical considerations, but also in order to optimize a variety of physicochemical properties. It is beyond the scope of this article to discuss at length the variation of these properties with electrolyte composition. Here

only general principles will be mentioned. For details, the reader is directed to the monograph by Strelets (2).

Table 4 displays the physicochemical properties of the most common constituents of the electrolyte along with those of molten elemental magnesium (39,40).

TABLE 4. Physicochemical properties of liquid magnesium and electrolyte components.

Metal or Chloride	Properties						
	Melting Point (K)	Temperature (K)	Vapor Pressure (torr)	Density ($g.cm^{-3}$)	Electrical Conductivity ($ohm^{-1}.cm^{-1}$)	Viscosity (cP)	Surface Tension ($dyn.cm^{-1}$)
Mg	924	974	6.67	1.577	4.405×10^4	1.250	541.5
$MgCl_2$	987	1037	2.35	1.654	1.110	1.958	66.36
KCl	1043	1093	1.04	1.499	2.287	0.965	96.02
NaCl	1073	1123	0.85	1.530	3.745	0.938	110.65
$CaCl_2$	1055	1105	-	2.059	2.257	2.494	143.35
$BaCl_2$	1235	1285	-	3.140	2.215	4.192	-
LiCl	883	933	0.08	1.480	5.973	1.294	126.03

The melting temperature of the electrolyte, or more precisely its liquidus temperature, ideally should be lower than the melting point of magnesium, 651°C, if the metal is to be harvested in the liquid state. This eliminates the need to superheat the cell beyond the degree necessary to prevent magnesium from freezing and thus minimizes metal losses through evaporation, oxidation, and dissolution in the molten salt. Furthermore, an electrolyte with a low solidus temperature takes longer to freeze when a power failure occurs. Thus, when a salt with a high melting point is added to improve certain properties, care must be taken not to increase the liquidus temperature to an unacceptable level. On the other hand, an electrolyte with a very low liquidus temperature is more apt

to penetrate the refractory cell liner at cell operating temperatures and thus shorten the cell life. All things considered, it seems that the electrolyte should have a liquidus temperature very close to the melting point of magnesium. This points to the need for multicomponent phase diagrams and explains the reason for the interest in such items as the phase diagram of the quarternary system, $MgCl_2$-KCl-NaCl-$CaCl_2$, reported recently (41).

The thermal stability of the electrolyte is inversely related to vapor pressure. In Table 4 all vapor pressures are given at a temperature of 50 K above the respective melting point. Although this exceeds the typical cell operating temperatures in some instances, all salts in Table 4 are molten under the stated conditions and thus their properties can be compared. In all cases the vapor pressures of these one-component melts are acceptably low for commercial electrolysis. These values of vapor pressure decrease when the salts are mixed with one another to form the multicomponent electrolyte. The vapor pressure of $MgCl_2$ is especially reduced through the formation of complex ions, which will be discussed later.

The density of the electrolyte must also be considered. Ideally the electrolyte should be as dense as possible in order to promote the buoyancy of the molten magnesium. Table 4 reports densities of pure salts. However, the density of a solution does not necessarily scale linearly with composition, particularly in complex-forming melts such as those containing $MgCl_2$. Table 4 shows that one of the roles of $CaCl_2$ in the electrolyte is to increase its density. In cells operating without $CaCl_2$ in the electrolyte the concentration of $MgCl_2$ is not allowed to drop below a certain level; otherwise the densities of magnesium metal and electrolyte become close enough that their separation is unacceptably slow. The addition of $BaCl_2$ to increase density has also been reported (2,42).

Cells containing electrolyte based on LiCl have been proposed, and several electrolyte compositions patented (42,43). Molten magnesium is denser than the electrolyte in these cells and sinks to the cell bottom. Such cells have not found commercial application for a number of reasons. LiCl is an expensive reagent, and with its strong affinity for water complete dehydration is energy intensive. There are difficulties associated with separating the metal from the sludge which also sinks to the cell bottom, and with directing the metal to the collection point. However, a closed cell, properly designed, carefully operated, fed with high quality anhydrous feed, should be able to avoid the sludging problem and produce metal successfully.

Electrical conductivity is arguably the most important property of the electrolyte. The voltage gradient in the interelectrode space, which in turn has a pronounced effect on the electrode separation distance, the dissipated heat, and the specific expenditure of energy, depends most strongly on the electrical conductance of the cell. Electrical conductivities for the individual electrolyte components are given in Table 4. NaCl and LiCl improve electrical conductivity which, being a transport property, is closely related to the structural characteristics of the melt. These will be discussed in the next section.

During electrolysis the applied voltage is higher than the decomposition potential calculated by equation (57) which is derived on the assumption of equilibrium: kinetic factors give rise to overpotentials. The applied voltage may be expressed (44) as

$$V_{cell} = E_{MgCl_2} + (\eta_a + \eta_c)_{cathode} + (\eta_a + \eta_c)_{anode} + \eta_{electrodes} + \eta_{ohmic} \quad (60)$$

where E_{MgCl_2} is the reversible or equilibrium decomposition potential given by equation (57) and is a function of composition and temperature; η_a is the activation overpotential at the electrode and is a function of composition, temperature, and current density; η_c is the concentration overpotential at the electrode and is a function of composition, temperature, and current density; $\eta_{electrodes}$ includes the potential drops due to rectification and the resistances associated with bus bars, electrodes, and electrical contacts between them; and η_{ohmic}, the ohmic overpotential or IR drop, is due to the electrical resistance of the electrolyte itself and is proportional to current density and interelectrode distance and inversely proportional to the electrical conductivity of the electrolyte and to the electrode area.

The activation and concentration overpotentials, confined to the electrode area, are related to the deposition mechanism and will be discussed later. Regarding the IR drop, it should be noted that in molten salts, in contrast to aqueous systems, the ohmic overpotential can be significant, amounting to as much as 40% of the total cell voltage.

Figure 5 shows schematically the distribution of the individual voltage components, which are a function of total cell current and consequently depend on cell size and design. Only recently has this information been reported in the literature (45). For a nominal 100 kA anhydrous cell operating at current densities from 0.8 to 1.3 A cm^{-2}, the cell voltage lies between 6.0 and 7.5 V. Curiously, the ohmic overpotential of the electrolyte, while substantial, seems

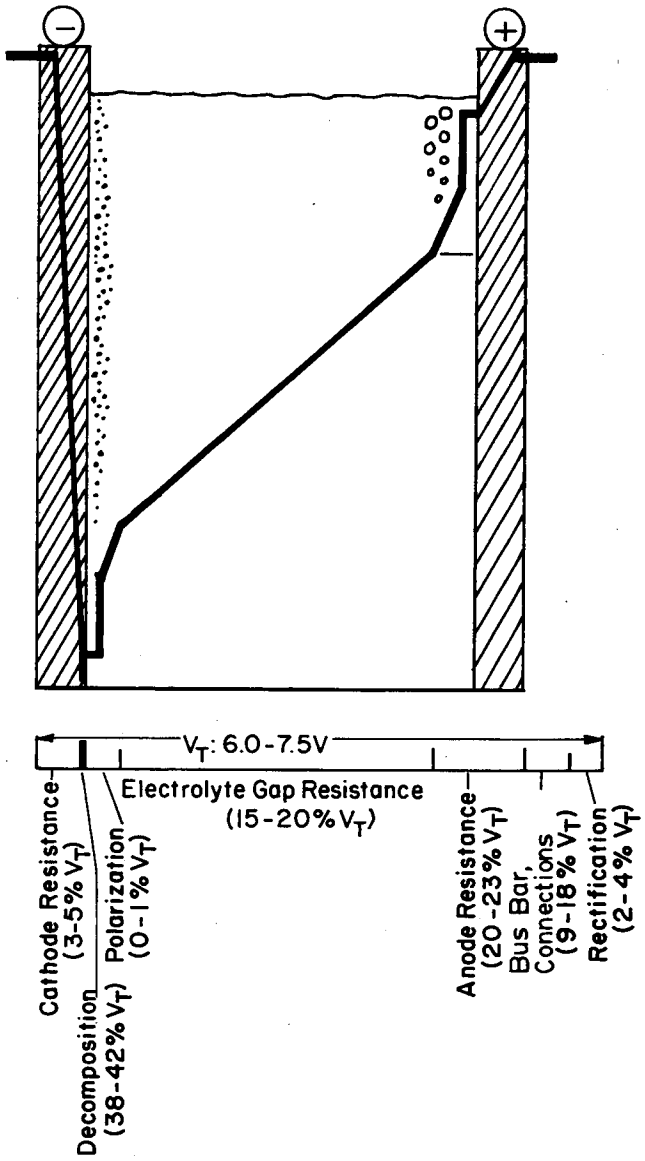

Figure 5. Overpotential distribution in a magnesium electrolysis cell.

surprisingly low compared to that encountered in Hall-Heroult aluminum electrolysis cells. This may be due in part to differences between magnesium and aluminum practices with respect to cell geometry and operating conditions.

Generally speaking, electrolysis cells are capital efficient at high current density and energy efficient at low current density. In other words, the higher the current density, the greater is the yield for a given reactor. However, as equation (60) shows, the higher the current density, the greater is the cell voltage and hence the farther removed from the thermodynamic minimum requirement. Over the years the magnesium industry has accumulated a vast body of knowledge related to process control and optimization.

Of all the components of the cell voltage, $\eta_{electrodes}$ and η_{ohmic} are the two that can be expected to be reduced. The reduction of the first requires development of suitable materials and will be discussed in a later section.

Reduction of the ohmic drop across the electrolyte at a constant production rate or current density requires that the specific electrical conductivity of the electrolyte be increased or that the interelectrode distance be decreased. The former may be achieved by altering the composition of the electrolyte subject to the other physicochemical requirements such as density and liquidus temperature as explained above. Decreasing the interelectrode spacing makes it more likely that the cell products, magnesium and chlorine, come into contact with each other and recombine through direct chemical reaction. This so-called recombination reaction decreases current efficiency, loosely defined as the molar ratio of metal product to electrical charge furnished by the power supply. In a magnesium cell operating at 100% current efficiency, it takes 2 coulombs of charge to reduce 1 mole of $MgCl_2$ to produce 1 mole of magnesium metal and 1 mole of chlorine gas. A second problem associated with decreasing the interelectrode gap is that the cells rely upon the generation of Joule heat to maintain temperature and thus keep the electrolyte from freezing. Given the range of electrical conductivity of electrolytes employed in current cell designs, there is a minimum interelectrode gap, reportedly 3 cm (5). Cells currently have interelectrode gaps of 6 to 7 cm.

Regarding heat generation, the high cell voltage given by equation (60) results in high specific energy consumption, since the two are related through the following equation (see ref. (42)):

$$W/P = V_{cell}/a.CE \qquad (61)$$

where W/P is the specific energy consumption, V_{cell} is the applied cell voltage, CE is the current efficiency, and a is a constant.

Finally, due to high ohmic overpotential, heat is generated. This is in turn dissipated according to

$$Q = I(V_{cell} - E) + (1 - CE)E.b.I \qquad (62)$$

where b is a constant.

The first term in equation (62) represents the heat due to ohmic resistance; the second term is the portion of the current efficiency loss that is converted to heat. Equations (60)-(62) indicate the need to decrease the ohmic overpotential or to increase the electrolyte conductivity by the addition of highly conductive salts.

In selecting the composition of the electrolyte it is also important to consider its viscosity, since the separation of liquid metal from the electrolyte is facilitated when the latter is less viscous. The viscosities of the individual electrolyte components are given in Table 4. As with other transport properties the formation of complex ions, such as those found in $MgCl_2$-containing melts, gives rise to negative deviations from additivity.

Finally, the surface tension of the electrolyte is also of concern. First, the electrodeposited magnesium metal should wet the cathode, and secondly, liquid magnesium should be well wetted by the electrolyte, otherwise the cathodic overvoltage will be high. In view of the high surface area of the small liquid magnesium droplets produced by electrodeposition, interfacial phenomena cannot be ignored. The surface tensions of the individual electrolyte components are given in Table 4. Impurities present in the melt generally affect the electrolysis process most significantly through alteration of the surface properties of the deposited magnesium metal droplets. For example, oxygen and sulfur are known to change the surface tension of liquid metals dramatically (46). At the same time, magnesium is an excellent getter of both oxygen and sulfur, and will extract them from oxides and sulfates present in the electrolyte. Should this occur the magnesium fails to wet the cathode, and the droplets do not coalesce. This in turn increases their vulnerability to recombination with chlorine and hence reduces current efficiency. Recently (47) it was reported that the ability of magnesium to wet the steel cathode increases with current density up to a value of 1.2 A cm^{-2}. Perhaps under these conditions the fast kinetics of deposition minimize the detrimental effect of

oxygen.

CaF_2 is present in small amounts in the electrolyte. At one time this was to counter the adverse effects of boron (12,48), modern cell feed preparation includes boron removal. However, CaF_2 is still added principally to help the coalescence of metal droplets and the wetting of the cathode surface thereby improving the recovery of magnesium. CaF_2 acts by fluxing the oxide film which will form if the electrolyte becomes contaminated with moisture. As well, CaF_2 seems to reduce the amount of cell mud formed, perhaps by increasing the capacity of the electrolyte to dissolve oxides.

2.2.3 Structural characteristics

Evidence in the literature suggests that $MgCl_2$ does not exist as Mg^{2+} cations and Cl^- anions when dissolved in alkali chloride melts; instead, these solvents act as ligand donors, and magnesium finds itself coordinated in the form of anionic complexes. This has profound effects on the thermodynamic and transport properties of $MgCl_2$. Attempts to elucidate melt structure have been made by indirect methods of investigation, thermodynamic and electrochemical, and by direct spectroscopic methods.

2.2.3.1 Cryoscopy and calorimetry

The binary phase diagrams of $MgCl_2$-ACl, where A is an alkali metal, have been determined (49-53). In all systems there is the formation of intermediate compounds, shown schematically in Figure 6 and summarized in Table 5. The trend in the melting points of the compounds suggests that their stability increases with the size of the alkali-metal cation. Alternatively, CsCl is a better ligand donor than LiCl.

Førland (55), in an attempt to rationalize the shape of the liquidus line on the magnesium chloride-rich side of the binary systems $MgCl_2$-KCl and $MgCl_2$-NaCl, proposed a model in which the melt contains two types of chloride ions: those attached to two magnesium ions thereby bridging them (-Cl-), and those connected to only one magnesium ion (-Cl). Additional alkali chloride is then dissolved according to the reaction

$$\begin{array}{c} | \quad | \\ \text{-Mg-Cl-Mg-} \\ | \quad | \end{array} + A^+Cl^- = 2(\text{-Mg-Cl}) + A^+ \qquad (63)$$

Using the above equation to calculate the concentration of magnesium chloride in the melt, Førland was able to generate the $MgCl_2$-KCl liquidus. In the

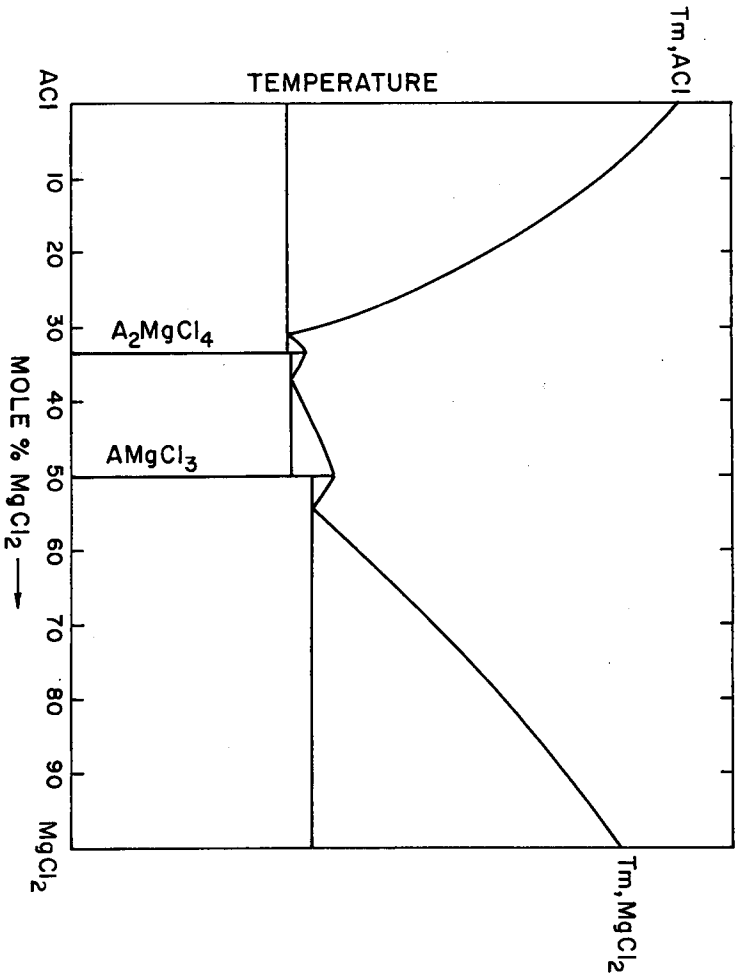

Figure 6. Phase diagram of the binary system ACl-$MgCl_2$ (schematic).

TABLE 5. Phase diagram data for binary $MgCl_2$ - ACl systems.

Binary System	Compounds & Melting Points (K) $MgCl_2$:ACl 1:3	1:2	1:1	3:1	Reference
$LiCl-MgCl_2$	[no compounds: complete solid & liquid miscibility]				49
$NaCl-MgCl_2$		(Na_2MgCl_4) 758	$(NaMgCl_3)$* 738		50
		(Na_2MgCl_4) 748	$(NaMgCl_3)$ 741		51
$KCl-MgCl_2$		K_2MgCl_4	$(KMgCl_3)$		52
		K_2MgCl_4 704	$KMgCl_3$ 758		51
$RbCl-MgCl_2$		Rb_2MgCl_4 750	$RbMgCl_3$ 823		53
$CsCl-MgCl_2$	Cs_3MgCl_5 800	Cs_2MgCl_4 818	$CsMgCl_3$ 883	$(CsMg_3Cl_7)$ 838	54

* parentheses denote incongruently melting compounds

$MgCl_2$-NaCl system the effort was less successful.

Flood and Urnes (56) studied freezing point depression on the alkali chloride-rich side of the binary systems, $MgCl_2$-KCl, $MgCl_2$-NaCl, and $MgCl_2$-RbCl. The cryoscopic behavior was explained by assuming that all $MgCl_2$ present is completely complexed according to the reaction

$$2A^+ + 2Cl^- + MgCl_2 = 2A^+ + MgCl_4^{2-} \quad (64)$$

This model succeeded in predicting the liquidus on the alkali chloride-rich side of the binary phase diagrams up to 30 mole% $MgCl_2$, but failed to rationalize the liquidus on the magnesium chloride-rich side. Both studies assumed ideal Temkin behavior since thermodynamic data were not available.

Calorimetric studies of these systems by Kleppa and McCarty (57) showed that the assumption of ideality is far from valid since rather large heats of mixing were measured. Furthermore, the interaction parameter $\lambda = \Delta H^M/X(1-X)$, where ΔH^M is the integral heat of mixing and X is the mole fraction, shows a strong composition dependence with a pronounced minimum at the composition corresponding to that of the complex compound A_2MgCl_4. As shown in Figure 7, the magnitude of the minimum increases in the order Li < Na < K < Cs. The appearance of the minimum was rationalized in qualitative terms by a modified version of the conformal solution theory developed by Davis (58).

2.2.3.2 Thermodynamic models

Additional information about melt structure can be obtained by the measurement of partial thermodynamic properties of the binary $MgCl_2$-ACl systems, principally by emf studies of formation cells (36,59,60,61). The measured emf data from all studies seem to be in good agreement with each other, although there is disagreement over their interpretation.

As a modification of the Flood and Urnes model, Neil et al. (36) proposed that the complex species formed according to equation (64) dissociate by the reation

$$MgCl_4^{2-} = Mg^{2+} + 4Cl^- \quad (65)$$

On the basis of emf measurements, the equilibrium constant of reaction (65) was calculated to be 1.8×10^{-3} at 800°C in the KCl-$MgCl_2$ system. Such a low value of the dissociation constant was taken to be an indication of the high stability of the $MgCl_4^{2-}$ ion. Their assumption of Temkin ideality, contrary to previously reported calorimetric data, was criticized by Ikeuchi and Krohn (61), who used their own data to obtain the concentration dependence of the partial entropy of mixing of $MgCl_2$ and concluded that the complex species dissociate according to equation (65), although not in the quantitative terms proposed by Neil et al. (36).

The data mentioned above were used by Pelton and Thompson (62) to demonstrate the quantitative success of their structural model for $MgCl_2$-containing melts. They also assumed that complex $MgCl_4^{2-}$ anions are formed. The complexing, however, according to the reaction

$$Mg^{2+} + 4Cl^- = MgCl_4^{2-} \quad (66)$$

is partial, and takes place even in pure $MgCl_2$. Under this assumption the melts of $MgCl_2$-ACl always contain Mg^{2+}, A^+, $MgCl_4^{2-}$, and Cl^-, which mix randomly. Quantitative agreement with the experimental data is obtained by this model

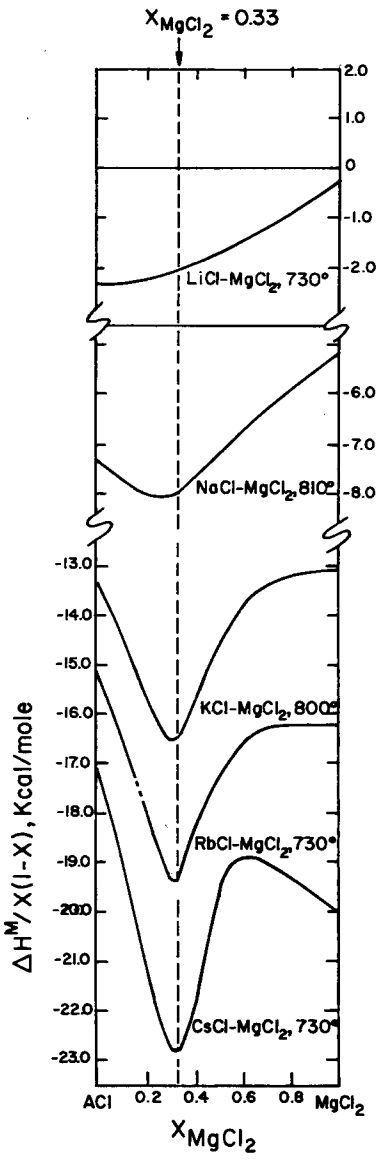

Figure 7. Concentration dependence of the interaction parameters for the binary $MgCl_2$-ACl system.

using two adjustable parameters: one independent of the alkali metal cation and therefore constant for the whole family of $MgCl_2$-ACl systems, and one depending on the alkali metal cation.

The conclusion drawn from the thermodynamic studies reviewed here is that the behavior of the thermodynamic properties is consistent with the assumption that there is a complex species present in melts of alkali chlorides containing magnesium chloride.

2.2.3.3 Spectroscopy

Braunstein (63) criticized the previous quantitative thermodynamic treatments of binary molten salt systems containing magnesium chloride, and noted that the development of quantitative relations between the association constants and the activity coefficients should be supported by independent evidence of the structures of the associated ionic species. Spectroscopic studies can provide such evidence.

Table 6 presents a summary of the results obtained by Raman spectroscopy. Early studies (64) suggested the presence of $MgCl_6^{4-}$ units in molten $MgCl_2$ and $MgCl_3^-$ in melts of KCl-$MgCl_2$. In subsequent studies (65-68) the spectra of the melts were interpreted in terms of a residual ionic lattice, which implies the presence of polynuclear aggregates of the formula $(MgCl_2)_n$. X-ray diffraction studies of single crystals of K_2MgCl_4 and Cs_2MgCl_4 (72) indicated that the former is tetragonal and the latter is orthorhombic, composed of distinct $MgCl_4^{2-}$ species in which magnesium is tetrahedrally coordinated to chlorides Recent Raman spectroscopic investigations by Brooker and co-workers (69-71) found that $MgCl_4^{2-}$ is the predominant species in melts of composition, $MgCl_2 \cdot 2ACl$, while a fraction of magnesium exists in the form of polynuclear aggregates, probably of the formula $Mg_2Cl_6^{2-}$. This direct spectroscopic evidence supports the presence of the complex $MgCl_4^{2-}$ as the dominant species in magnesium chloride-containing melts, as was suggested by the earlier thermodynamic studies. The predominance of $MgCl_4^{2-}$ in concentrated melts does not exclude the presence in small amounts of other species such as $MgCl_3^-$, which has been recently observed (73) in solutions of divalent magnesium in basic KCl-$AlCl_3$. An equilibrium reaction

$$MgCl_4^{2-} = MgCl_3^- + Cl^- \qquad (67)$$

has been proposed to explain the formation of $MgCl_3^-$ in these melts Figure 8 shows the Raman spectra of polycrystalline $MgCl_2$ at 298 K and molten $MgCl_2$ at 1000 K. These spectra were obtained as part of a spectroelectrochemical

TABLE 6. Raman spectra of $MgCl_2$-containing melts.

System (reference)	Temperature (K)	Raman Frequencies (cm^{-1})*	Comments about Structure
$MgCl_2$ (s) (ref. 64)	305	242±3(s,P)	presence of $MgCl_6^{4-}$
$MgCl_2$ (ℓ) (ref. 64)	1003	269±7 (m) 241±5 (m) 214±12 (m,b) 142±7 (w)	
$MgCl_2$-KCl (s) (ref. 64)	305	450? 248±5 (w) 210±7 (vw) 152±7 (vw)	existence of $MgCl_3^-$ pyramidal configuration (C_{3V})
$MgCl_2$-KCl (ℓ) (ref. 64)	798	451±6 (vwD) 250±6 (mP) 208±5 (mD) 158±6 (wP)	
$MgCl_2$-2KCl (s) (ref. 64)	305	452? 252±5 (w) 235±6 (vw) 200±7 (w) 154±7 (vw)	
$MgCl_2$-2KCl (ℓ) (ref. 64)	798	450±5 (wD) 255±5 (mP) 232±5 (vw?) 198±6 (wD) 152±7 (vwP)	

*Abbreviations: s=strong; m=medium; w=weak; vw=very weak; b=broad; P=polarized; D=depolarized.

TABLE 6 (continued)

System (reference)	Temperature (K)	Raman Frequencies (cm^{-1})*	Comments about Structure
$MgCl_2$-KCl (ℓ) (ref. 65)	823	282±5 (P) 255±2 (P) 233±6 (P) 221±3 (P) 163±5 (D) Values averaged Cl^-/Mg^{2+} ratios of 3.0, 3.6, and 4.0	$\nu_1 MgCl_n^{(2-n)}$ $\nu_1(A_1)$ $MgCl_4^{2-}$ $(MgCl_2)_n$ polymer $(MgCl_2)_n$ polymer Cl-Mg-Cl bending modes
$MgCl_2$-KCl (ℓ) (ref. 66)	823	256 (s,P) 227 (b,P) 160 (b,D)	distribution of polynuclear $MgCl_n^{(2-n)}$ aggregates
$MgCl_2$-KCl (ℓ) (ref. 67)	723	252±2 (P) 100±3 (D) 330±3 (D) 142±5 (D)	$MgCl_4^{2-}$ tetrahedral species
$MgCl_2$ (s) (ref. 68)	295	243 (s) 157 (w)	D_{3d}^5 space group for solid $MgCl_2$
	673	236 (s) 146 (w)	
	873	233 (s) 140 (w,b)	
	973	231 (s) 136 (w,b)	
$MgCl_2$ (ℓ) (ref. 68)	1023	195 (s,b,P) 102 (w,b)	residual lattice bands in the melt

*Abbreviations: s=strong; m=medium; w=weak; vw=very weak; b=broad; P=polarized; D=depolarized.

TABLE 6 (Continued)

System (reference)	Temperature (K)	Raman Frequencies (cm^{-1})*	Comments about Structure
K_2MgCl_4 (s) (ref. 69) Single crystal	77	77 103 140 195 213	coordination number changes from 6 to 4 upon melting
K_2MgCl_4 (ℓ) (ref. 69) Single crystal	1050	115±5 145±3 227±5 252±1 350±5	
Cs_2MgCl_4 (s) (ref. 69)		90 106 145 267 366 382	discrete $MgCl_4^{2-}$ tetrahedral units in both solid and melt
Cs_2MgCl_4 (ℓ) (ref. 69)		104±3 142±3 225±5 250±1 350±5	
$MgCl_2$ (s) (ref. 70)		155 240	discrete $MgCl_4^{2-}$ tetrahedral species in equilibrium with polynuclear complexes of unknown structure
$MgCl_2$ (ℓ) (ref. 70)	1010	100 130 140 194 244 335	

*Abbreviations: s=strong; m=medium; w=weak; vw=very weak; b=broad; P=polarized; D=depolarized.

TABLE 6 (Continued)

System (reference)	Temperature (K)	Raman Frequencies (cm^{-1})*	Comments about Structure
$MgCl_2$ + nACl (ref. 71)	873-973	Vary with n and ACl	discrete $MgCl_4^{2-}$ species, also $Mg_2Cl_7^{3-}$ present at high concentrations of $MgCl_2$

*Abbreviations: s=strong; m=medium; w=weak; vw=very weak; b=broad; P=polarized; D=depolarized.

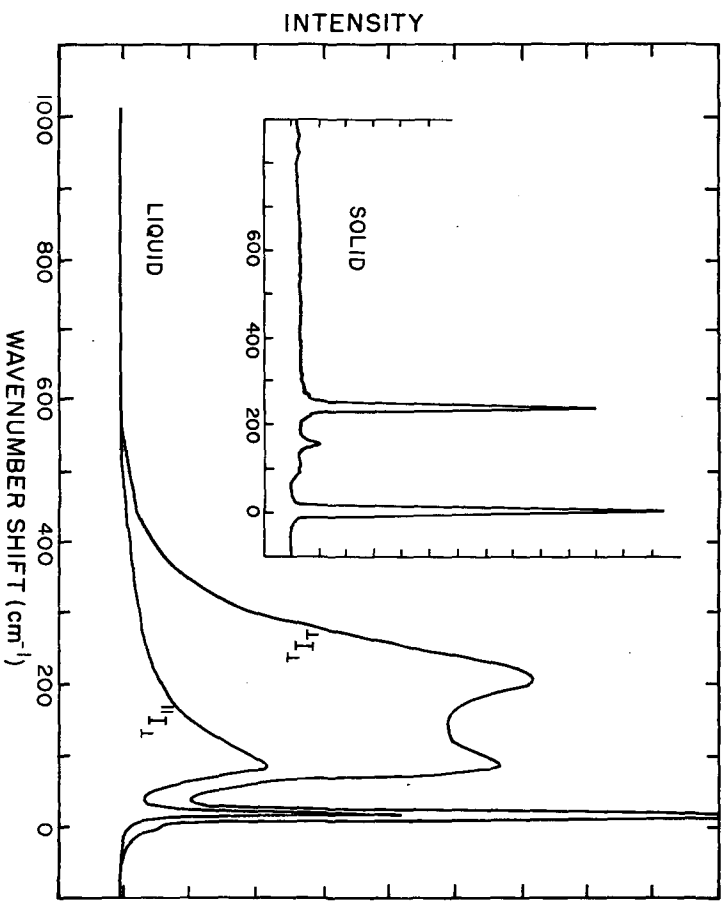

Figure 8. Raman spectra of polycrystalline $MgCl_2$ at 298 K and molten $MgCl_2$ at 1000 K.

investigation of laboratory-scale light metal electrolysis cells (34,74,75).

The Raman spectrum of an electrolyte of the industrial composition 11% $MgCl_2$, 6% $CaCl_2$, 65% NaCl, and 18% KCl, is shown in Figure 9, along with the spectrum of pure molten $MgCl_2$. There is a shift in the main $MgCl_2$ peak from 205 cm^{-1} in pure $MgCl_2$ to 249 cm^{-1} in the industrial electrolyte. The presence of the strong peak in the latter could serve as the basis for continuous monitoring of melt composition (75).

2.3 Industrial Electrolysis Cells

An electrolysis cell is a device that causes electrical energy to perform chemical work, which in the case of magnesium production is the decomposition of $MgCl_2$ into magnesium metal and chlorine gas according to reaction (51). This occurs by the transfer of electrical charge between two electrodes immersed in the electrolyte. At the negatively charged cathode, electrons are transferred to magnesium cations, which are thereby reduced to neutral metal atoms. Liquid magnesium droplets form. At the positively charged anode, chloride ions transfer electrons to the electrode and are thereby oxidized. Chlorine gas evolves as bubbles on the anode. As these reactions proceed the electrolyte is depleted of magnesium chloride, which must be periodically added to the melt. One important statistic that is often overlooked is the ratio of chlorine to magnesium produced in the cell: 2:1 on a molar basis but 5500:1 on a volumetric basis! One might argue that these cells are primarily chlorine cells which happen to make magnesium as a by-product.

The electrolysis cell, having produced molten magnesium and chlorine gas, must keep them separated from one another so that they do not recombine and undo the work of electrolysis, and so that each can be conveniently removed from the cell. The problem of keeping the cell products apart is nontrivial because both magnesium and chlorine are fluids, and both are buoyant in all the industrial electrolytes in use today. Recombination can be prevented either through the use of physical barriers or by control of the electrolyte circulation patterns. Physical barriers are effective; however, they increase the cell resistance and thus the required applied cell voltage. This leads to higher energy consumption. Control of circulation patterns requires that the cell components be dimensionally stable. This is difficult to achieve over long periods of time. For example, even in anhydrous electrolytes there is a small amount of residual oxygen which reacts with the anode, slowly consuming it.

The characteristics of the various electrolytic cells are given in Table 7, which was constructed from published data. It should be pointed out, however,

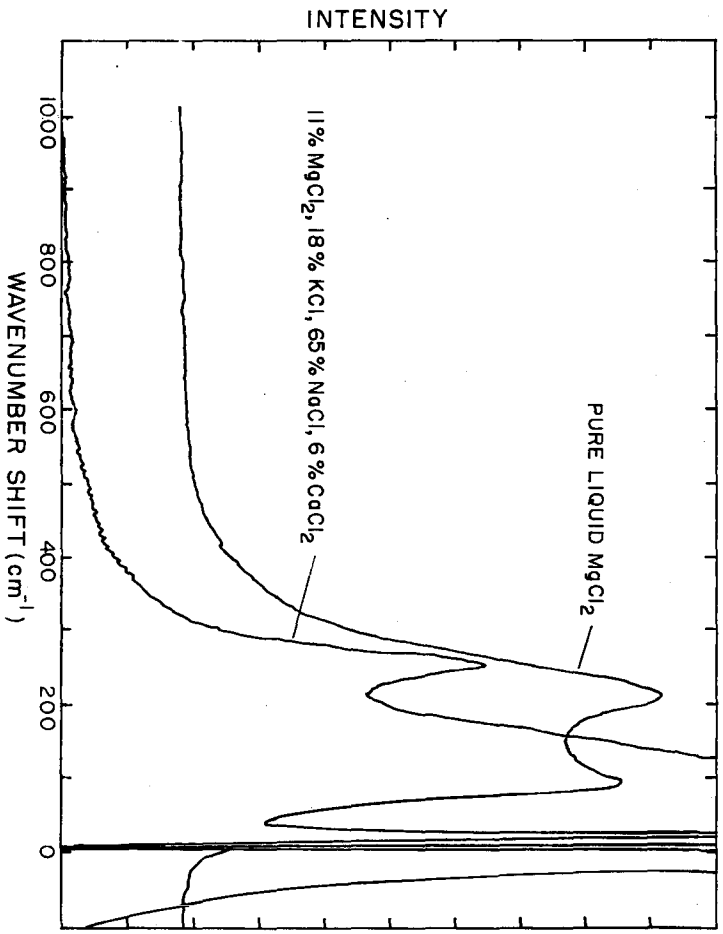

Figure 9. Raman spectra of molten pure $MgCl_2$ and of an electrolyte composed of 11% $MgCl_2$, 6% $CaCl_2$, 65% NaCl, and 18% KCl.

TABLE 7. Characteristics of magnesium electrolysis cells.

	Dow	I. G. Farben
Cell body	steel	steel, ceramic lining
Ampere load, maximum (kA)	150	100
Voltage per cell (V)	6.5	6.0 - 7.5
Cathode efficiency (%)	80+	90+
Energy efficiency (%)	30	34
Anode-cathode spacing (cm)	4	6 - 7
Energy consumption, (kWh/kg Mg)	18	12 - 14
Operating temperature (°C)	700	740
Graphite consumption (g/kg Mg)	100	15
Mg content (%)	99.8	99.8
Method of heating	external	internal resistance
Cell feed (%)		
$MgCl_2$	72 - 75	96.3
$CaCl_2$	0.5	1.4
NaCl	1.0	2.2
MgO	<0.5	0.1
H_2O	-25	0.1
C	-	0.1
Cell sludge (%)		
Mg	2 - 3	0.5 - 2
$MgCl_2$	20	5 - 15
MgO	20	5 - 15
Oxides	-	1 - 15
Carbon	-	0.1 - 1

that these data may not be fully representative of actual industrial practice. The metals industry operates in a very competitive environment, and many details, particularly those related to cell design and engineering, are not public knowledge. The same is true for accurate specific energy consumption values. What follows, then, is an attempt by the authors to interpret the available information and explain the electrochemistry of industrial electrolytic operations.

2.3.1 Anhydrous (I. G. Farben - Norsk Hydro - VAMI)

The striking feature of these cells is the hood-like semi-wall which surrounds the anode, forming a chlorine collection compartment where a negative pressure is maintained without allowing air to leak in from outside the cell. The purposes of this structure are to separate the products of electrolysis and to remove chlorine gas from the electrolyte. The semi-wall is made of acid chamotte or fused alumina, chosen not only to act as a barrier to chlorine but also to prevent the conduction of electric current. Figure 10 illustrates a series of electrode assemblies which are the smallest operational units of an I. G. Farben cell. The assembly consists of an anode compartment surrounded by two cast steel cathodes whose construction is shown in a side view. The cell is a steel tank lined with refractory insulation and contains four or five electrode assemblies set in a sealed cell cover and immersed side-by-side in the electrolyte. The cell may also contain a pre-cathode which is used to electro-purify the bath prior to actual magnesium production. Pre-electrolysis is usually conducted at a current density of 0.5 A cm^{-2}.

During electrolysis chlorine bubbles form on the anode and rise to the electrolyte surface in the anode box out of which chlorine gas is vented along a common duct. Chlorine evolution, in conjunction with small local density variations in the electrolyte due to depletion of magnesium chloride, sets up a pumping action which forces the electrolyte to circulate through the cathode slots in a motion depicted in Figure 10. Molten magnesium metal forms on the cathode, wets it, and coalesces into droplets. The combination of buoyancy due to the density difference between the metal and the electrolyte and forced convection of the electrolyte due to so called "gas lift" off the anode causes the magnesium to flow upwards to the top edge of the cathode face plate from which it is directed to the metal collection compartment. Magnesium droplets are swept along. These droplets coalesce and eventually, due to density differences, rise to the surface of the electrolyte in the space between the electrode assemblies. The bath circulation also acts to deliver fresh

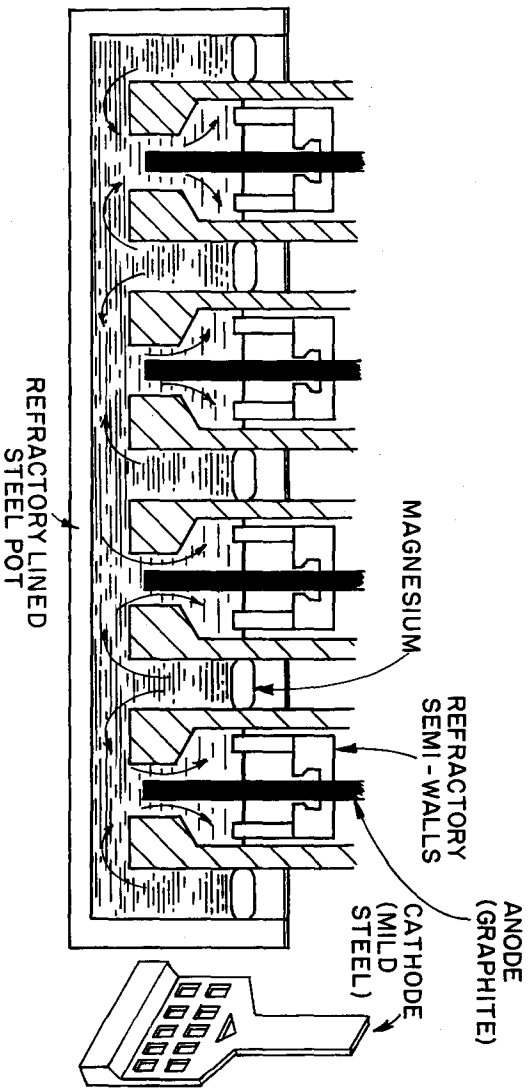

Figure 10. Cell for anhydrous magnesium chloride electrolysis (schematic).

electrolyte containing magnesium chloride to the interelectrode space. The large anode-cathode distance, reportedly up to 14 cm, effectively separates the cell products and, consequently, results in high current efficiency. This design, however, imposes limits on the current density. The cells are self-heating, i.e., the Joule heating of the electrolyte keeps the system at temperature. If the interelectrode gap is reduced too much in order to decrease the energy consumption inadequate heat will be generated, and the melt will freeze. An energy balance in this cell has been reported (42); energy efficiency is about 34% (13).

The cell is charged with anhydrous molten $MgCl_2$ containing approximately 4% $CaCl_2$ and NaCl. The latter two components are not electrolyzed, and over time they accumulate and cause the melt level to rise. Some cells are charged continuously, others periodically. Once weekly the melt level is regulated by leveling, which is the removal of excess electrolyte, and smutting, which is the removal of the sludge from the bottom of the cell. In addition to electrolyte components this sludge contains MgO, finely dispersed Mg droplets (so-called "fish eggs"), SiO_2 from the lining, other oxides, and carbon. The source of carbon is the anodes which can crack due to salt penetration.

Metalling, i.e., harvesting molten magnesium metal, is performed as needed, typically one to four times daily. The metal must be removed from each electrode assembly. In the Dow cell, discussed in the next section, all the product metal is led to a common collection point, an advantage over the I. G. Farben cell.

Cell performance is governed to a large extent by the performance of the anode compartment. The most common problems arise from failure of the refractory semi-wall due to thermal shock caused by sudden variations in melt level. To avoid the attendant cell shutdowns, melt levels must be closely controlled, ideally to the point of total automation.

In order to eliminate the problems caused by semi-wall failure diaphragmless cells have been developed. In such cells magnesium metal is directed in one of two ways: first, by inverted troughs to the front of the cell where there is a common receiver separated from the main electrode compartment by a wall to prevent recombination; secondly, by melt circulation. In the former case these diaphragmless cells resemble Dow cells described below in Section 2.3.2.

2.3.2 Hydrous (Dow Chemical)

Hydrous electrolytic cells are used exclusively by the Dow Chemical Company and account for 35% of the world's production of magnesium. From an operational

viewpoint the salient features are external heating, adjustable anodes, and the use of a cell feed containing up to 25% H_2O in crystalline form. As a consequence of the latter, the anode gas is not marketable chlorine and need not be strictly confined. Indeed, there is no semi-wall separating anode and cathode. Furthermore, the interelectrode distance can be reduced and is limited only by the need to avoid chemical recombination of the cell products and by the density of suspended particulates. As well, there are more anode-cathode pairs in a reactor of a given size as compared to an anhydrous cell. The cell resistance is lower than that of anhydrous cells: the Dow cell can be operated at higher currents.

The reported (12,48) graphite consumption (given in Table 7) suggests that most of the water content of the cell feed is removed at or near the melt surface, probably during the charging operation. In this sense the cell may be viewed as being composed of two chambers. In the front chamber water is flashed under conditions that suppress hydrolysis, reaction (11): HCl gas is present. In the electrolysis chamber the decomposition of magnesium chloride takes place in an electrolyte still containing substantial amounts of water. The hydrolysis reaction, however, cannot be completely suppressed, and the oxychloride formed is decomposed according to reaction (20) to produce MgO and HCl. The large amount of sludge which is removed from the cell (13), reportedly 180-320 kg per 1000 kg of magnesium produced, supports the deduction regarding hydrolysis. As mentioned in Section 2.1.4, hydrolysis can also occur by reactions (49) and (50) which consume the graphite anode as a source of carbon and the anodic cell product as a source of chlorine in order to form HCl.

The cell consists of a steel container to which a series of conical steel cathodes have been welded, as shown in the schematic of Figure 11. Just below the melt level the steel container is lined with a refractory material. Between 20 and 30 anodes, each the shape resembling that of a giant sharpened pencil, pass through a refractory cover which centers them so that they are aligned concentrically with their respective cathodes. The anodes are composed of graphite of relatively high quality both in terms of mechanical strength and chemical purity. Periodically the anodes are lowered in order to adjust their position with respect to the cathodes. Cell feeding is also conducted periodically. The electrolyte is kept molten by externally heating the bottom of the steel container in a gas-fired refractory chamber. The external heating provides the flexibility of being able to restart the operation after power interruption even for extended periods of time. According to early reports (76)

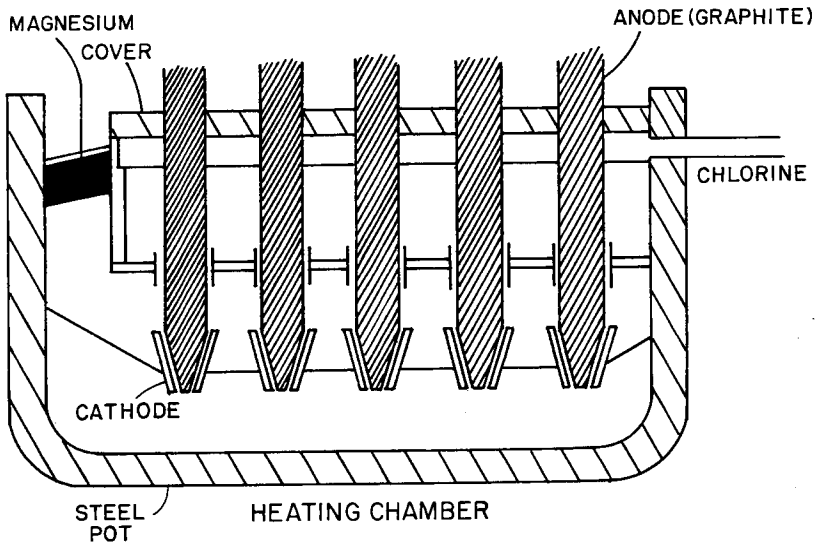

Figure 11. Cell for hydrous magnesium chloride electrolysis (schematic).

this design was chosen because of the frequent power interruptions in the Midland, Michigan area where the first cell was installed.

During operation the cell remains tightly sealed under moderate vacuum. A popping sound can be heard, probably hydrogen burning, and a yellow flame is visible. Air is introduced into the ducting outside the cell to remove the evolving cell gases which when diluted contain about 4% Cl_2, 4% HCl, 1% H_2, and 1% CO_2, and are used to produce HCl in a hydrochloric acid furnace.

Magnesium metal product is directed to a common sump. It had been reported earlier (76) that this was done by a separate system of inverted troughs which capture the metal as it is produced at the conical cathodes. Recent information (13) suggests that the inverted troughs are themselves part of the conical cathodes and part of the cathodic shell. As the magnesium droplets rise they coalesce.

It appears that the engineering aspects of internal cell configuration, including the feeding system, and the physical separation of magnesium metal

from the evolving chlorine, are of great importance to the successful operation of the Dow cell.

An energy flow diagram for the entire process has been constructed (77): the energy efficiency is 29.5%, the plant efficiency about 10.5%, and the thermal efficiency based on total energy consumption of fossil fuel is about 6.5%.

2.4 Mechanism of Magnesium Electrodeposition

2.4.1 Reasons for loss of current efficiency

The mechanism of electrodeposition of magnesium will be discussed with reference to the anhydrous electrolytic process for which the electrode configuration is better known. In the hydrous Dow process the presence of crystalline water complicates the electrochemistry: water here will be discussed in the context of an impurity.

An enlarged simplified version of the electrode assembly of the anhydrous cell is shown in Figure 12(a). The overall reaction is that given by equation (51), while the individual electrode reactions may be written as follows:

$$\text{cathode:} \quad Mg^{2+} + 2e^- = Mg(\ell) \tag{68}$$

$$\text{anode:} \quad 2Cl^- = Cl_2(g) + 2e^- \tag{69}$$

Magnesium deposits at the cathode in the form of liquid metal droplets whose size, typically between 1 and 2.5 mm (78,79), depends upon current density. The average time required for the droplets to detach and rise to the melt surface in the metal collection compartment has been estimated (78) to be about 30 seconds.

Chlorine is produced at the anode in equimolar quantities to magnesium. Chlorine bubbles are typically 0.35 to 2.00 mm in diameter (80). Based on measurements of rise rates it is estimated that a chlorine bubble reaches the melt surface in the anode compartment in about 10 seconds under typical operating conditions. At low current densities the bubbles rise up the anode and expand in response to the decrease in hydrostatic pressure. At higher current densities the bubbles detach from the anode before reaching the melt surface.

Cathode current efficiency is normally about 85% or 90% for carefully regulated cells. The chlorine yield, i.e., anode efficiency, is even lower, reportedly about 93-94% of the magnesium yield, or 80 to 85% in absolute value.

Evidently there is a loss of current efficiency of about 15% which has not been explained quantitatively. The possible mechanisms are summarized as

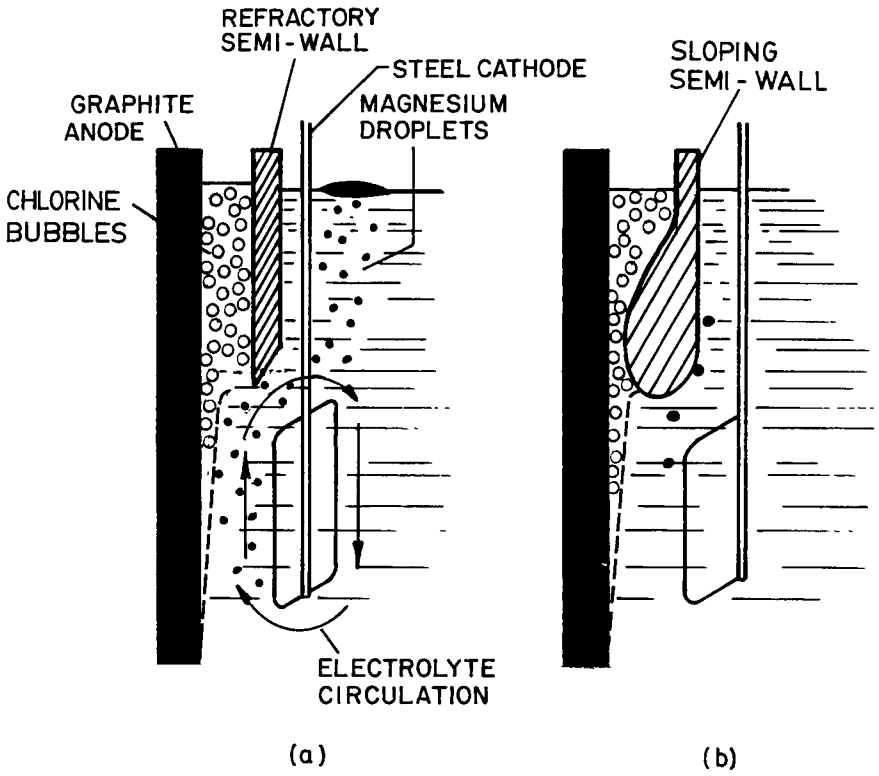

Figure 12. (a) Electrode assembly of anhydrous cell.
(b) Proposed improved electrode assembly.

follows:

I. Parasitic reactions involving simultaneous discharge of ions, i e., impurities, whose deposition potential is not as negative as that of magnesium,

II. Redox reactions involving multivalent ions of impurity metals or perhaps even magnesium itself,

III. Direct recombination of the products, i.e , magnesium droplets reacting directly with chlorine bubbles to form magnesium chloride,

IV. Indirect recombination of the products, i.e., magnesium metal dissolved in the electrolyte reacting with chlorine dissolved in the electrolyte to form magnesium chloride,

V. Failure of magnesium droplets to coalesce with the consequence that the metal becomes dispersed in the electrolyte, reacts with impurities, and finally sinks to the bottom of the cell to become entrapped in the sludge.

VI. Burning of magnesium metal in the metal collection compartment where it contacts air. The MgO that forms can be found in the sludge and even entrapped in the metal product.

There is no agreement among various investigators as to which of the above mechanisms predominates It seems, however, that all mechanisms operate simultaneously and are interrelated in a manner that at present is not well understood. Visual observation of laboratory scale cells has revealed the following, however. Electrolytes containing hydrolysis products such as dispersions of MgO or MgOHCl appear cloudy or milky Such electrolytes turn clear when treated with $SOCl_2$ (34), presumably due to the chlorination of the oxide. With the onset of electrolysis a brown cloud (34,81,82), or "streamer"-like growth from the cathode, can be seen. Some refer to this phenomenon as metal fog. Furthermore, during electrolysis, the electrolyte next to the electrode becomes colored. An explanation of these phenomena has been proposed and will be presented later. Another observation that may be related to loss of current efficiency is that after electrolysis small dispersed magnesium droplets are found at the bottom of the cell. These are covered with a black film, probably a sub-oxide (34,81), or perhaps an iron boride.

2.4.2 The role of impurities

Impurities are detrimental to the operation of the cell and reduce the current efficiency through mechanisms I and V.

The electrolyte contains small amounts of water which is presumed to be

present as hydroxychloride. The exact composition and structure of the species are unknown.

The electrochemical behavior of H_2O in KCl-$MgCl_2$ has been studied by cyclic voltammetry (83). Consideration was given to possible electrochemical reactions such as

$$H_2O + Mg^{2+} + 2e = H_2(g) + MgO(s) \quad (70)$$

$$OH^- + Mg^{2+} + e = \tfrac{1}{2}H_2(g) + MgO(s) \quad (71)$$

The above reactions demonstrate the doubly detrimental effect of the presence of water. First, hydrogen deposition at the cathode consumes electrons intended to produce magnesium; secondly, the insoluble MgO at the cathode surface leads to its passivation as evidenced by the observed cathodic polarization (83). Furthermore, the presence of a growing MgO layer on the cathode may be a factor in preventing the coalescence of magnesium droplets. This in turn leads to loss of current efficiency by mechanism V. It was found (83) that MgO could be reduced and the deposition of Mg restarted by highly cathodic polarization.

The chemical effect of water is to hydrolyze $MgCl_2$ according to the reaction

$$MgCl_2 + H_2O = MgOHCl + HCl \quad (72)$$

which is analogous to reaction (19).
Hydrolysis, however, is moderated by the presence of alkali chlorides, as evidenced by comparative measurements in pure molten $MgCl_2$ and $MgCl_2$-KCl systems (83). Perhaps the complexing of $MgCl_2$ affords some measure of protection and slows the kinetics of hydrolysis (see also Section 2.1.2).

Solubility of magnesium oxide in chlorides is very low. The solubility product of MgO in CaO-$CaCl_2$ at 850°C was found to be $\sim 10^{-6}$ (83). The system CaO-$CaCl_2$ is important to the electrolytic recovery of magnesium, since it is believed that MgO is introduced into the electrolyte by the hydrolysis of $CaCl_2$ followed by metathetical reaction of CaO with $MgCl_2$

$$CaCl_2 + H_2O = CaO + 2HCl \quad (73)$$

$$MgCl_2 + CaO = MgO + CaCl_2 \quad (74)$$

It has been suggested (2) that MgO is transferred by electrophoresis to the cathode where the passivation effects discussed above then occur. More recently, MgO has been found to be carried along with the bulk circulation of the electrolyte (84). During periods of intensive circulation, it is claimed that the relatively smaller and lighter MgO particles are lifted from the cell sludge and are partly deposited by adhesion forces on the cathode surface. The nature of the adhesion forces is not described. MgO also affects the anodic process, since it may be chlorinated, forming CO_2 which dilutes the anodic gas. Carbochlorination may also occur, thereby consuming the anode itself.

CaF_2 is added to the electrolyte to dissolve the MgO films that form on the cathode and over the magnesium droplets (85). This has the added beneficial effect of changing the surface tension of the melt so as to improve wetting of the electrode and thereby reduce cathodic overvoltage.

Effects similar to those caused by MgO are also caused by the presence of sulfates. Having a decomposition potential of about -3.40 V at 700°C (2), sulfate ions cannot be readily electro-oxidized. Their detrimental effects derive mainly from the following reactions (86,87):

$$3Mg + Mg^{2+} + SO_4^{2-} = 4MgO + S \quad (75)$$

$$4Mg + Mg^{2+} + SO_4^{2-} = 4MgO + MgS \quad (76)$$

Reaction (76) indicates that the cathode is passivated by a film composed of MgO and MgS. The sulfur produced by reaction (75) causes the electrolyte to foam and thus impairs melt circulation. The importance of the latter to good separation of magnesium from chlorine has been discussed above.

Salts of iron, titanium and manganese reduce current efficiency through a combination of mechanisms II and III. It has been reported (2) that when the electrolyte contains 0.1 to 0.5% iron no magnesium metal production occurs. Furthermore, due to so-called redox looping the melt is never depleted of iron. One representation involves metallothermic reduction of trivalent iron by the reaction

$$2FeCl_3 + Mg = 2FeCl_2 + MgCl_2 \quad (77)$$

followed by anodic oxidation of divalent iron by the reaction

$$Fe^{2+} = Fe^{3+} + e^- \quad (78)$$

Similar reactions can be written for titanium and manganese.

Anhydrous electrolytic processes do not seem to suffer from the presence of iron salts since the chlorination step at or above 1050°C in preparing $MgCl_2$ removes virtually all the volatile iron chloride. The feed for the hydrous electrolytic process undergoes no analogous processing. Thus, iron must be treated in a different fashion, perhaps by precipitation in the early aqueous feed preparation stages or in the melt through the addition of a transition metal oxide which reacts metathetically to form a volatile transition metal chloride and iron oxide. The latter precipitates out of solution into the sludge, which is known to contain iron.

Reaction of magnesium with the lining can also form impurities according to

$$SiO_2 + 4Mg = Mg_2Si + 2MgO \quad (79)$$

which represents substantial metal loss. Evidence for reaction (79) is the presence of SiH_4 detected in the vent gases. This may be attributed to the reactions

$$Mg_2Si + 2H_2O = SiH_4 + 2MgO \quad (80)$$

$$Mg_2Si + 4HCl = SiH_4 + 2MgCl_2 \quad (81)$$

The most deleterious effects in terms of metal losses are caused by the presence of <u>boron</u> in the electrolyte. Reportedly (2,76) each 10 ppm (parts per million) of boron in the cell feed causes a 1% reduction in current efficiency. In spite of the fact that more than 70% of the boron in the cell feed vaporizes as boron chloride in the anode gas, as little as 0.015% boron in the electrolyte can cause the current efficiency to drop to 50%. Although the detrimental effect of boron was recognized as early as 1895 (88), the mechanism of breakdown is still a matter of dispute. Some feel (2) that boron forms, by deposition, a strong cathode-passivating film, while others (76) believe that its effect is due to its reaction with magnesium to form metallic borides. This metal-like deposit coats the rising droplets exerting a dispersing action on the metal and preventing coalescence.

A polarographic study (89) conducted with an electrolyte containing 5% NaCl, 5% KCl, and 90% $MgCl_2$ showed that the action of boron depends on the applied current density. As shown in Figure 13 there is a series of waves which were interpreted as boron discharge with nucleation on the cathode of the elementary compounds of boron at lower current densities and discharge of MgB_2-type compounds at higher current densities. Recent studies (90) of electrodeposits obtained from other $MgCl_2$-based electrolytes tend to support these findings.

2.4.3 <u>The recombination reaction</u>

Loss of current efficiency may be attributed to the recombination reaction which occurs by mechanism III or IV.

The first mechanism is <u>direct</u> reaction of chlorine bubbles and magnesium droplets, both rising in the electrolyte but of different sizes and rising at different velocities. The recombination reaction under these conditions is represented by the equation

$$Mg(\text{liquid droplets}) + Cl_2(\text{gas bubbles}) = \underline{MgCl_2}(\text{dissolved in electrolyte}) \quad (82)$$

The back reaction will occur via equation (82) if the cell design does not provide for effective separation of magnesium droplets and chlorine bubbles. However, even if the products of electrolysis come in contact, there is a kinetic barrier to reaction (82), since magnesium metal is well wetted by the electrolyte, and the chlorine bubbles will have to penetrate this encapsulating electrolyte film before any reaction can occur. Regardless, the cell must be constructed to prevent magnesium from being trapped in the anode compartment.

In order to study the fluid mechanics of the anhydrous cell, Ukshe et al. (80) developed a physical model based on an aqueous solution of 10% $NaNO_3$ which matched closely the known values of the kinematic viscosities and surface tensions of the industrial electrolytes. Operation of the cell was simulated by a supply of nitrogen gas and oil droplets representing the evolution of chlorine and magnesium, respectively. This study indicated that separation of anode and cathode products in the existing magnesium cells is unsatisfactory due to entry of magnesium into the anode compartment followed by its eventual chlorination. A cell design that included sloping semi-walls which are claimed to improve separation was proposed (80) and is shown in Figure 12b. This work also pointed to the value of comparative aqueous-molten salt studies in determining similarity criteria. Such results could also aid the development of the science of scale-up of electrolysis cells.

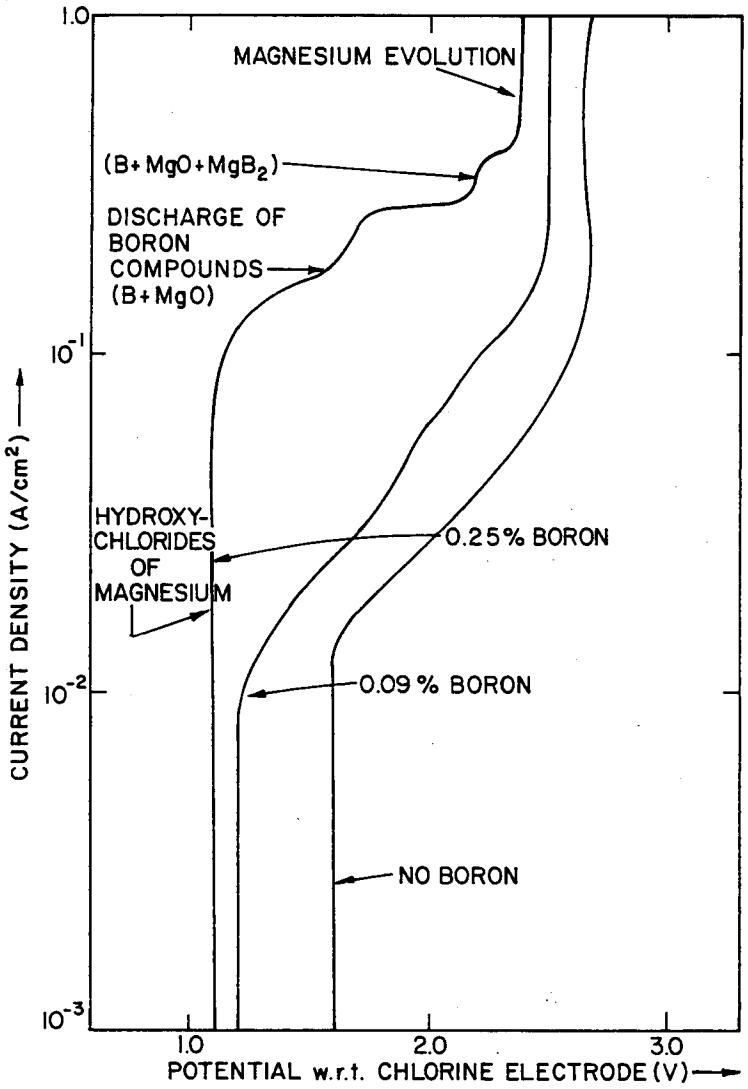

Figure 13. Polarogram of 90% $MgCl_2$, 5% NaCl, 5% KCl melt with boron impurity additions.

The second mechanism for the recombination reaction is the reaction between magnesium and chlorine, both dissolved in the electrolyte.

$$\underline{Mg} + \underline{Cl_2} = \underline{MgCl_2} \qquad (83)$$

where the underline denotes solution in the molten salt phase. In reaction (83) the form and extent of dissolution of magnesium and chlorine in the electrolyte are important. In this regard solubility-reducibility studies have been conducted. Bukun and Ukshe (91,92) investigated the weight loss of magnesium metal immersed in melts hermetically sealed in steel containers. The content of magnesium in the reacted electrolyte was determined by the amount of evolved hydrogen when the reacted electrolyte was dissolved in acidified water. The reaction is

$$Mg + 2H_2O = Mg(OH)_2 + H_2 \qquad (84)$$

It was found that magnesium reacts even with melts that do not contain magnesium chloride, while for melts containing $MgCl_2$ the extent of reaction, other conditions being the same, increases with $MgCl_2$ content. Temperature plays a role: higher temperatures result in higher solubility. Chemical solubility of magnesium in the electrolytes was considered in terms of the following reactions:

$$Mg + Mg^{2+} = 2Mg^{+} \qquad (85)$$

and

$$Mg + Mg^{2+} = Mg_2^{2+} \qquad (86)$$

Both reactions imply the formation of monovalent magnesium ions which may exist as the monomer Mg^{+} or the dimer Mg_2^{2+} or as a mixture of the two. Formation, however, of monovalent ions may result in the onset of redox looping. The deposition potentials have been estimated (92) to have the following values at 800°C:

$$E^{\circ}(Mg/Mg_2^{2+}) = -2.36 \text{ V} \qquad (87)$$

and

$$E^\circ(Mg_2^{2+}/Mg^{2+}) = -2.84\ V \qquad (88)$$

Van Norman and Egan (93) used anodic chronopotentiometry to study the solubility of magnesium metal in its molten chloride and interpreted their results in terms of equation (86). However, their solubility data were lower than those previously obtained (92) by a factor of 2 to 3. Krumpelt et al. (94) also interpreted their equilibrium solubility data in terms of reaction (86). The chemical solubility of magnesium in $MgCl_2$ at 750°C is about 0.15 mole %.

Another mode of dissolution of magnesium has been proposed: dissociation into the cation and two electrons by the reaction

$$Mg = Mg^{2+} + 2e^- \qquad (89)$$

where the electrons are solvated, i.e., they behave as anions. Some authors refer to them as liquid phase F-centers. The association of solvated electrons with divalent magnesium cations to form subvalent magnesium species is difficult to distinguish from the reaction products of equations (85) and (86). The formation of streamers and melt coloration are both thought to originate from metal solubility.

Magnesium can also enter the electrolyte as a fine metal dispersion. This phenomenon has been studied in KCl-$MgCl_2$ melts during electrolysis (95,96). It was found that $BaCl_2$ and CaF_2 tend to inhibit dispersion, while MgO stabilizes the dispersed system.

Reaction (84), which is used for determining solubility of magnesium in the electrolyte, cannot differentiate between soluble and dispersed magnesium. This observation may be responsible for discrepancies in the solubility results.

Dispersed magnesium metal in the electrolyte may also cause loss of current efficiency by imparting some measure of electronic conductivity to the melt.

Using the solubility data obtained previously (91-96), Øye and co-workers (78,81,97,98) attempted to determine the rate-limiting step in the recombination reaction by developing a mass-transfer model based on a simplified cell. Chemical reaction, mass transfer, and collision between magnesium droplets and chlorine bubbles were eliminated. The model considered the dissolution rate of Cl_2 or Mg in the electrolyte to be the most probable rate determining mechanism. The success, then, of the model would be to predict residence times for

magnesium droplets and chlorine bubbles taking into account their sizes. However, previously reported solubility values were much too high. This prompted redetermination of magnesium solubility (98) by equilibrium reducibility experiments conducted in tantalum containers. With the new solubility data the proposed mass-transfer model indicated that the rate of formation of small magnesium droplets (<0.1 mm) in the electrolyte is the most likely rate determining step in the recombination reaction.

Finally, the cathodic deposition process of magnesium in electrolytes composed of $CaCl_2$-NaCl was investigated by Tunold (82) using transient electrochemical techniques. Among the cathode substrates were platinum, steel, carbon, and magnesium itself. The conclusion was that magnesium deposition is mainly diffusion controlled although slightly mixed with a heterogeneous reaction, which in this case is probably the electrode reaction.

More promising techniques of investigation for elucidating the mechanism of electrodeposition in molten salts are those combining electrochemical and spectroscopic methods, often referred to as spectroelectrochemical techniques. For example, Raman scattering studies of laboratory scale magnesium electrolysis cells containing electrolytes of industrial composition and operating at industrial current densities have been reported (34,74,75).

3. THERMOCHEMICAL METHODS OF MAGNESIUM PRODUCTION

Non-electrolytic methods of magnesium production are all based upon the thermochemical reduction of magnesium oxide which is obtained by processing any one of a number of magnesium resources, e.g., magnesite ($MgCO_3$), dolomite ($MgCO_3 \cdot CaCO_3$), or olivine ($(Mg, Fe)_2SiO_4$). The prototypical reaction is

$$MgO + X = Mg + (XO \text{ or a compound containing Mg, X, and O}) \qquad (90)$$

where X, the reductant, can be carbon, a metal, a metallic alloy, or a metallic compound such as a carbide or silicide.

Magnesium has a high affinity for oxygen; magnesium oxide is extremely stable ($\Delta_f G^\circ = -493$ kJ per mole MgO at 1000 K (21)). Figure 14 illustrates the temperature dependence of the equilibrium between magnesium and magnesium oxide along with metal/metal-oxide equilibria for other metals of interest in the present discussion. Such plots of the variation of the standard free energy of reaction with temperature are called Ellingham diagrams and are constructed on the basis of a fixed quantity of oxidant, in this case one mole of oxygen. The

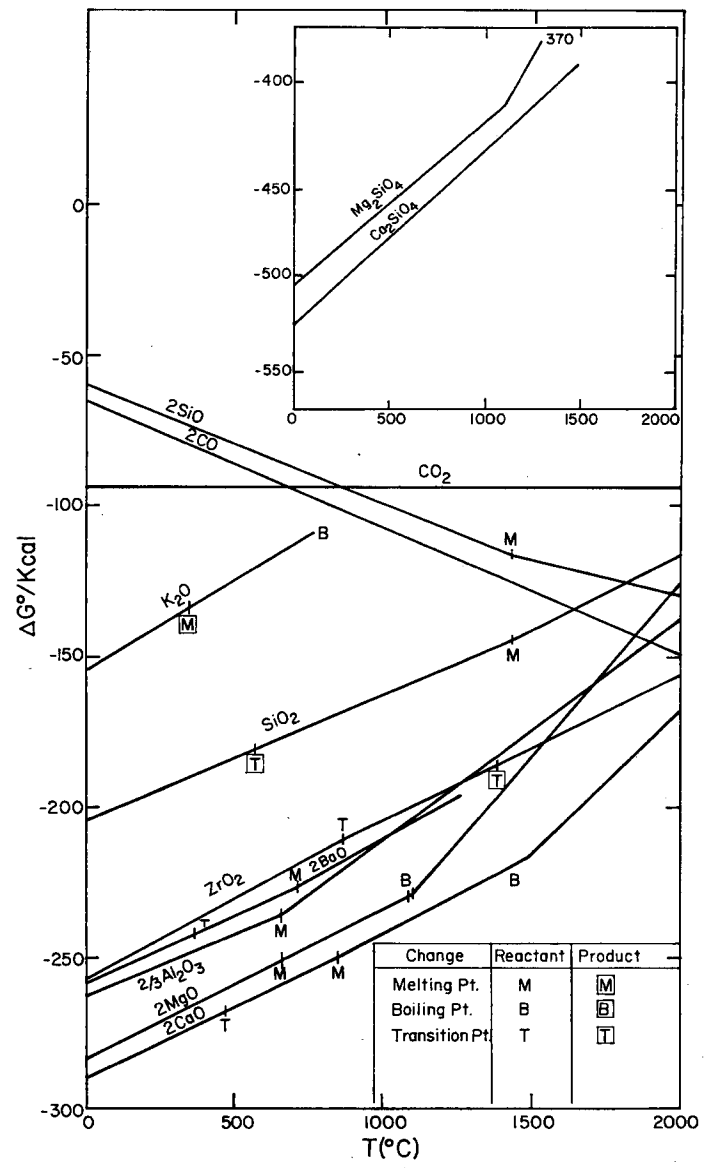

Figure 14. The temperature dependence of the standard free energy of formation of selected oxides and silicates of importance to metallothermic production of magnesium.

result is that the diagram ranks the various reactants in order of their chemical affinities for the common oxidant. The noblest metals appear at the top of the diagram; the stablest oxides appear at the bottom. Metathetical reactions can be easily assessed. For example, MgO is stabler than Al_2O_3; thus, molten magnesium at 800°C can be expected to attack alumina. This is not evident when the standard free energies of formation of alumina and magnesia are compared, as they are typically quoted per mole of oxide: at 1000 K, $\Delta_f G^\circ(Al_2O_3)$ = -1.36 MJ per mole of Al_2O_3 (21). From the information given in Figure 14 it seems that thermochemical reduction of MgO is possible only by reaction of the oxide with elemental calcium. However, the Ellingham diagram (99) presents thermodynamic data for reactions in which all species are in their standard states, i.e., solid phases in their stable crystallographic modification and gases at unit fugacity. Changes from standard conditions can alter the thermodynamics significantly and make possible reactions that appear forbidden at first glance.

The Ellingham diagram is generic and can be constructed to rank relative affinities for any oxidant. There are diagrams for sulfides, halides, and carbides (100-102). In this chapter, to explain the chemistry of silicothermic reduction, part of an Ellingham silicate diagram has been constructed from available thermodynamic data.

3.1 Carbothermic Reduction

Figure 14 shows that at 1854°C, carbon monoxide becomes stabler than magnesium oxide: at higher temperatures carbon, the commonest reducing agent in chemical metallurgy, will directly reduce magnesium oxide by the reaction

$$MgO(s) + C = CO(g) + Mg(g) \qquad (91)$$

Reaction (91), which is termed carbothermic reduction, is favored over magnesium carbide formation. Kelly (25,26) using compiled thermodynamic data calculated the standard free energy of reaction to be

$$\Delta G^\circ_{76} = 155{,}810 - 100.34T + 3.401T\ln T + 0.51\times10^{-3}T^2 - 2.088\times10^{5}T^{-1} \qquad (92)$$

The critical problem in carbothermic reduction arises from the fact that magnesium is produced as one component of a two-component gas phase. The separation of magnesium vapor from carbon monoxide is a formidable task under these conditions. Condensation of molten magnesium is one approach. However,

as the gas mixture is cooled below 1854°C reaction (91) proceeds to the left. Substantial losses of magnesium product are incurred. Nevertheless carbothermic reduction has been used in plants in Permanente, California and Konan, Korea during periods of high demand for the metal.

The reaction is performed in 600 kVA electric furnaces. The details of the operation are described in the literature (103,104). By the use of jets of natural gas, the reaction products are shock-chilled in order to minimize the parasitic effects of back reaction. As of this writing, this method is not being used commercially to produce magnesium.

3.2 Metallothermic Reduction

When the reductant in reaction (90) is a metal or metal alloy, the reaction is termed metallothermic reduction. Of the metals treated in Figure 14, only calcium appears to be suitable as an elemental reductant. However, this is true only when all four species of reaction (90) are in their standard states. The equilibrium can be shifted to the right by decreasing the chemical potentials of magnesium and XO. When magnesium vapor is produced its fugacity is decreased by operation at reduced pressure. The activity of XO is decreased by fluxing or slagging, i.e., the formation of a multicomponent liquid phase in which XO dissolves.

3.2.1 Reduction with silicon

When silicon is used as the reductant it is usually in the form of a metal alloy, typically ferrosilicon. Under these conditions reaction (91) can be written as

$$2MgO(s) + Si{\cdot}xFe(s) = 2Mg(g) + SiO_2(s) + xFe(s) \qquad (93)$$

By analogy, when magnesium is charged as calcined dolomite the reaction is

$$2MgO{\cdot}2CaO(s) + Si{\cdot}xFe(s) = 2\,Mg(g) + (CaO)_2{\cdot}SiO_2(s \text{ or } \ell) + xFe \qquad (94)$$

There are two technological approaches to silicothermic reduction, resulting in two distinct processes: externally heated vacuum retort (Pidgeon Process) and internally heated vacuum furnace (Magnetherm process).

3.2.1.1 The Pidgeon Process

The theoretical principles of silicothermic reduction of magnesium in externally heated vacuum retorts have been described by Pidgeon (105-107); others have treated the relevant technology (108-111). Recent commercial developments of the process have also been reported (112).

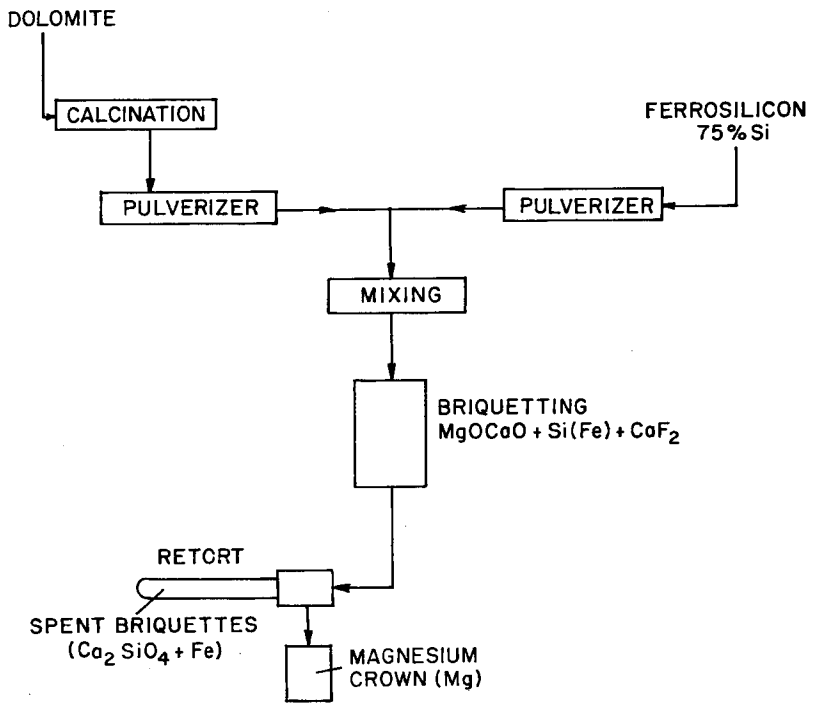

Figure 15. Flowsheet of the Pidgeon process (schematic).

Figure 15 shows a simplified version of the process flowsheet. The raw materials are dolomite and ferrosilicon. Dolomite containing at least 20 percent magnesium is calcined in rotary kilns at a temperature of about 1350°C. Ferrosilicon containing 75 percent silicon is obtained by carbothermic reduction of silica in the presence of iron in an electric furnace.

The finely ground raw materials, with a small addition of CaF_2, usually about 2.5 weight percent, are mixed and formed into hard, dense

briquettes. Since the externally supplied heat to the retort is transferred to the charge mainly by radiation, the briquette size and ability to withstand decrepitation become critical parameters in the operation.

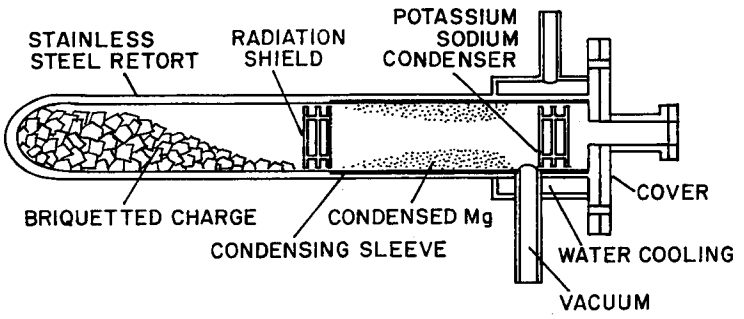

Figure 16. Pidgeon reactor (schematic).

A charging machine consisting of a wire mesh conveyor is used to distribute the briquettes along the length of the horizontal retort which is maintained at an operating temperature of about 1200°C. The retort, shown in Figure 16, is made of a seamless stainless steel tube 3 m long with a 28 cm bore diameter and a capacity of 160 kg of charge. The end of the retort is fitted with a steel sleeve in the extended water-cooled section for the condensation and collection of magnesium vapor. The end is plugged with a two-layer, eyed metal disk which has two purposes: it provides a means of withdrawing the sleeve at the end of the cycle, and it collects any sodium or potassium that might be present in the reaction vapors.

The operating cycle lasts approximately 10 hours and can be divided into three periods. Immediately after charging and before sealing, burnoff occurs, during which time any carbon dioxide and water in the charge are driven off. The low vacuum period follows sealing of the retort and completes the burnoff operation. Finally, the high vacuum period during which the pressure is maintained at 100-150 μm Hg lasts about 9 hours. The magnesium vapors produced are condensed in a crystalline crown form on the steel jacket which is

maintained by water cooling at about 250°C. At the end of the cycle the retort is opened and the magnesium crowns are removed from the steel jackets and sent for melting, while the residue of the reaction is removed from the retort by a pressurized air-vacuum system. Pressurized air is also used occasionally to restore the collapsed hot end of a retort. A variation of the process utilizing a refractory-lined steel retort has been studied (113).

Process efficiency has traditionally been expressed (106) in terms of silicon efficiency, which is defined as

$$Si_{eff} = \frac{\text{Mg collected} \times 100\%}{\text{Mg equivalent of Si present}} \qquad (95)$$

even for the cases in which silicon is present in excess.

Process parameters and their effects on silicon efficiency have been extensively studied (106). Dolomite used in the process should not contain more than 2 percent insoluble material, which consists in most cases of silica or magnesium silicates, since finely dispersed insoluble material has a deleterious effect on the reactivity of the calcine. Also of great importance is the presence of alkali metals which should be limited to 0.15 percent maximum in dolomite in order to prevent burning of the magnesium crowns due to incomplete separation. The presence of about 2 percent fluorspar (CaF_2) has a catalytic effect on silicon efficiency. It has been suggested that the catalytic effect is due to the formation of low melting eutectics around the solid grains (114).

Although the effects of the operational parameters on the yield of the process are well understood, the reaction mechanism is not. When CaO is not a major constituent of the charge, reaction (93) is a possible mechanism. However, the vapor pressure of magnesium as calculated from available thermodynamic data is too low for an industrial operation. Indeed, direct measurements (115) of the vapor pressure of magnesium were found to be much higher than those calculated with reaction (93). Better agreement between measured and calculated vapor pressures was found with the following reaction:

$$4MgO(s) + Si(s) = 2Mg(g) + Mg_2SiO_4(s) \qquad (96)$$

X-ray diffraction measurements of the reaction products support this. Formation of silicates has also been suggested by Kroll (116). Table 8 presents the results for a number of possible reactions.

TABLE 8. Equilibrium magnesium vapor pressures for thermochemical reduction of MgO.

Reaction / vapor pressure of magnesium	Reference
1. $4MgO(s) + Si(s) = 2Mg(g) + Mg_2SiO_4(s)$	115
*log P = -12,750/T + 8.925	
2. $2(CaO{\bullet}MgO)(s) + Si(s) = 2Mg(g) + Ca_2SiO_4(s)$	118
*log P = 13.853 - 12,636/T - 1.283 log T	
3. $2(CaO{\bullet}MgO)(s) + Si(Fe) = 2Mg(g) + Ca_2SiO_4(s) + Fe$	117
log P = -10,875/T + 8.918	
4. $4MgO(s) + 2Al(Si) = 3Mg(g) + MgAl_2O_4 + Si$	132
log P = -7,658/T + 7.071	
5. $4MgO(s) + 2Al(\ell) = 3Mg(g) + MgAl_2O_4(s)$	132
log P = -9,280/T + 8.665	
6. $12CaO(s) + 21MgO(s) + 14Al(\ell) = 21Mg(g) + 12CaO{\bullet}7Al_2O_3(s)$	132
log P = -8,754/T + 8.462	
7. $MgO(s) + CaC_2 = Mg(g) + CaO(s) + 2C(s)$	calculated
log P = 12.53 - 1.611 log T - 9,105/T	

* estimated from plotted data

Pidgeon and King investigated the reduction of calcined dolomite by ferrosilicon according to equation (94). Their values of magnesium vapor pressure were four times higher than those previously reported (115) for reaction (93). The authors did not consider the formation of calcium orthosilicate but considered three possible mechanisms: (a) silicon vapor reduction; (b) formation of volatile SiO; and (c) solid diffusion between the reactants.

Mechanisms (a) and (b) would involve the reaction of solid with vapor, for example

$$2MgO + 2CaO + Si = 2Mg(g) + 2CaO + SiO_2 \quad (97)$$

$$SiO_2 + Si = 2SiO(g) \quad (98)$$

$$2MgO + CaO + 2SiO(g) = CaO + 2SiO_2 + 2Mg(g) \quad (99)$$

$$2CaO + SiO_2 = (CaO)_2SiO_2 \quad (100)$$

although the overall effect is that of equation (94).

Mechanisms (a) and (b) suggest that the reduction reaction will proceed even if the reactants are physically separated and communicate only by the flow of a gas such as hydrogen. Such experiments were performed (117) with no observable reaction taking place. Thus mechanism (c), which involved reaction between solids, was suggested (117).

The formation of calcium orthosilicate was postulated by Schneider (118), who considered the reaction

$$2(MgO{\bullet}CaO)(s) + Si(s) = 2Mg(g) + Ca_2SiO_4(s) \quad (101)$$

and measured the vapor pressure of magnesium under these conditions. Their results confirm that the equilibrium vapor pressure of magnesium over reaction (101) was ten times greater than that over reaction (96), which in practical terms implies that the reduction of calcined dolomite is easier than that of calcined magnesite. Calculated values (119) are in very good agreement with experimental values, as shown in Figure 17. In addition to equation (101), the possible formation of Ca_3SiO_5 has been discussed (114). As shown in Figure 14, the orthosilicates of calcium and magnesium are very stable compounds; their formation completely reverses the apparently unfavorable thermodynamic conditions for the silicothermic reduction of magnesium.

Schneider et al. (120) proposed a mechanism in which the effective reducing agent is calcium silicide, $CaSi_2$, which forms at high temperatures by the exothermic reaction

$$4CaO + 5Si = 2CaSi_2 + Ca_2SiO_4. \quad (102)$$

Subsequent kinetic studies (121, 122) postulated a solid-solid and solid-gas mechanism involving SiO which was identified by X-ray diffraction techniques. In contrast, $CaSi_2$ as suggested by reaction (102) could not be positively identified (122).

Wynnyckyj and Pidgeon (123,124) studied extensively the thermodynamics of the Ca-Si and CaO-MgO-SiO_2 systems and reported that the vapor pressure of magnesium

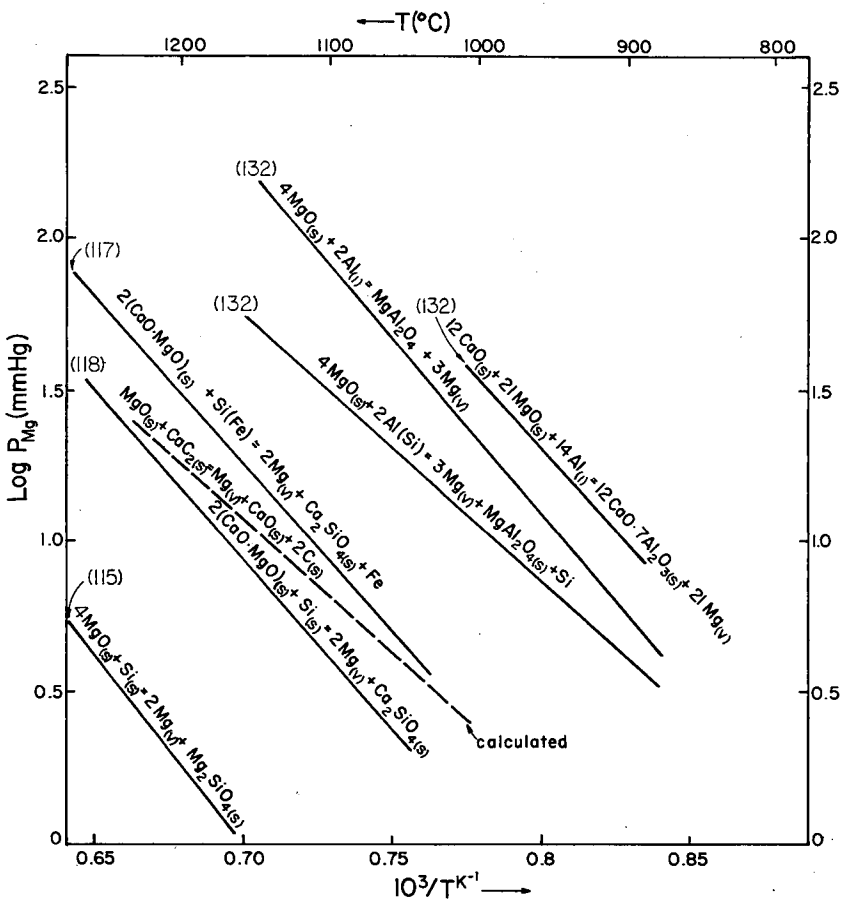

Figure 17. Vapor pressure of magnesium in the reduction of magnesium compounds.

is much higher than that predicted by equation (101) when the reductant, silicon, is in a state of reduced activity, e.g., when ferrosilicon is used instead of elemental silicon. That the vapor pressure of a product should increase as the chemical potential of a reactant decreases is an apparent contradiction. Certainly, the opposite is calculated (125) in the analogous system in which the reductants are aluminum and an aluminum-silicon alloy. The higher magnesium vapor pressure is reported over elemental aluminum.

3.2.1.2 The Magnetherm Process

Silicothermic reduction is also employed in the Magnetherm process, which was developed in France. The process surmounts the heat transport limitations imposed by the externally-heated Pidgeon retorts by effecting the reduction entirely in the liquid phase in a carbon-lined electrical furnace at high temperature (about 1600°C) and at reduced pressure (20-100 torr). Although the process is a batch-type operation, the hot raw materials are fed into the reduction furnace continuously, and the operation is computer-assisted and fully automated. Furthermore, magnesium is collected in the liquid state, another difference between the Magnetherm and the Pidgeon processes, and the raw materials are loaded from separate containers without mixing or briquetting.

A simplified schematic flow sheet of the Magnetherm process is shown in Figure 18. The evolution of the process has been described elsewhere (126-128) along with recent technological developments (129). Calcined dolomite containing 37% MgO is the magnesium resource, augmented with magnesite to bring the MgO content up to 39 - 39.5% equivalent. This is stored at a temperature of 600°C in a refractory-lined storage bin. Ferrosilicon, 77% Si, containing about 4% Al, is the reducing agent and is also stored in a bin over the reduction furnace.

Alumina, Al_2O_3, is used as a fluxing agent to form a molten slag and is obtained by the calcination of bauxite at 1200°C by the reaction

$$Al_2O_3 \cdot nH_2O(s) = Al_2O_3(s) + nH_2O(g) \qquad (103)$$

The presence of alumina in the calcium silicate slag also decreases the solubility limit of MgO, thereby reducing its loss by dissolution into this melt. The calcined bauxite containing 80% Al_2O_3 is stored in the appropriate bin from which it is fed directly into the furnace.

The raw materials for producing 1 tonne of magnesium ingot lie within the following limits:

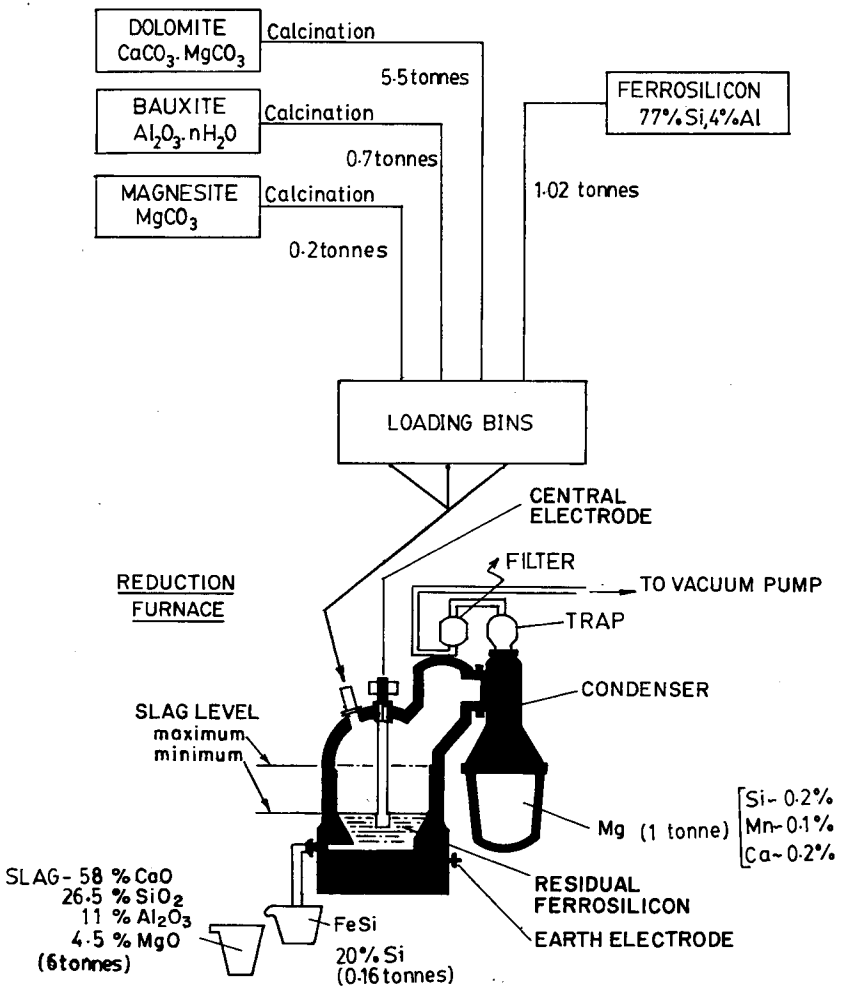

Figure 18. Flowsheet of the Magnetherm process (schematic).

dolomite (calcined): 5.5 tonnes bauxite (calcined): 0.7 tonnes

magnesite (calcined): 0.2 tonnes ferrosilicon (77% Si): 1.02 tonnes

The furnace consists of a cylindrical amagnetic steel shell lined internally with a refractory and thermally insulating lining, plus a layer of carbon blocks. The roof is made of a refractory-lined steel provided with three orifices, one connecting the furnace to the raw materials feed chute, the second, central orifice for inserting the graphite electrode, and the third through which the magnesium vapor escapes to the condenser. The roof is water-cooled to withstand the heat radiating from the surface of the slag. The bottom of the furnace contains the conducting hearth consisting of carbon blocks into which six water-cooled copper tubes serving as electrodes are sealed. The single-phase alternating current electrothermally heats the molten slag which acts as a resistor. The base of the furnace is also equipped with a tapping hole for removing slag and residual ferrosilicon. Furnaces presently in operation are rated at 5.5 MW, capable of producing 13 tonnes per day.

The condenser unit joined with a flange to the reduction furnace consists of a large diameter bent tube lined with refractory material in which the magnesium vapor condenses in the liquid state, a cast steel crucible for receiving the liquid magnesium, and a trap on the vacuum line from the condenser to prevent damage to the pumps.

Process control is achieved in part by an electronic system of weighing the raw materials and a computer controlled system designed to adjust the transformer ratio and hold the vacuum at the desired level. Furthermore, raw materials are analyzed by X-ray spectrometer and exit gases by mass spectrometer. These data are fed to a furnace control computer which then acts to maintain a constant slag composition of 4.5% MgO and 11% Al_2O_3. This is a definite advantage of the process over the Pidgeon process and to a great extent the basis for the strong competitive position that Magnetherm enjoys with the electrolytic processes.

The operation is discontinuous. There are two programmed daily operation cycles. At the beginning the furnace contains slag from the previous cycle to a depth of 1.5 m. The entire system is checked for leaks, the condenser is brought to the proper temperature, and the pre-set program regulates the feeding of the pre-heated raw materials. Calcined dolomite dissolves in the slag once its temperature reaches 1330°C. The reduction of dolomite then takes place according to the reaction

$$2(CaO{\cdot}MgO) + 2Si + nAl_2O_3 = SiO_2{\cdot}2CaO{\cdot}nAl_2O_3 + 2Mg(g) + \underline{Si} \quad (104)$$

at temperatures of 1600-1700°C and pressures of 20-100 torr. The underline denotes metal in solution. Of the products of reaction (104), magnesium metal escapes as vapor to the condenser while the involatile products, slag and residual ferrosilicon, remain in the furnace where, being immiscible, they separate. Ferrosilicon having a density (125) of 2.7 g/cm^3, slightly greater than that of the slag, forms globules which settle through it.

After eight hours of continuous feeding of raw materials the furnace is filled with slag to a depth of 2.4 m. The vacuum is replaced by inert gas at atmospheric pressure, operation is discontinued, and the transformer output is reduced to a level that compensates for heat loss. Tapping of the residual ferrosilicon and slag begins and lasts for an hour. Due to their immiscibility, residual ferrosilicon (20% Si) fills the tapping crucible while the slag overflows into a larger ladle and is granulated by water elsewhere.

Upon completion of a second similar cycle, the condenser crucible filled with magnesium is replaced by a clean condenser and an empty crucible during the slag tapping. The materials recovered per tonne of magnesium amount to 0.160 tonnes of residual ferrosilicon and 6 tonnes of slag consisting of 58% CaO, 26.5% SiO_2, 11% Al_2O_3, and 4.5% MgO. The energy consumption for the reduction is 9.5 kWh/kg of magnesium. Recent patents (130,131) claim that the use of low-cost aluminum skim in place of alumina reduces the energy consumption to 8.85 kWh/kg Mg and increases the production rate from 330 kg Mg/hr to 345 kg Mg/hr.

In preparation for a discussion of the thermodynamics of the Magnetherm process, equation (104) is rewritten below in a form that features the reduction of the magnesium oxide component of dolomite.

$$2MgO(s, \text{dolomite}) + Si(\ell, \text{metal}) = 2\,Mg(g) + SiO_2(\ell, \text{slag}) \quad (105)$$

which has as its standard free energy of reaction

$$\Delta G^\circ_{105} = 135{,}500 + 14.74T\log T - 102.7T \quad (106)$$

The relationship between the vapor pressure of magnesium and the activity of silicon in ferrosilicon can be calculated from the equilibrium constant

$$K_{105} = (P^2_{Mg} \cdot a_{SiO_2}) / (a^2_{MgO} \cdot a_{Si}) \quad (107)$$

Since ferrosilicon used in the Magnetherm process contains about 4% aluminum, a secondary reduction also occurs:

$$3MgO(s, \text{dolomite}) + 2Al(\ell, \text{metal}) = 3Mg(g) + Al_2O_3(\ell, \text{slag}) \quad (108)$$

for which the standard free energy is given as

$$\Delta G^\circ_{108} = 144{,}040 + 18.36T\log T - 134.88T \quad (109)$$

The equilibrium constant is

$$K_{108} = (P^3_{Mg} \cdot a_{Al_2O_3}) / (a^2_{Al} \cdot a^3_{MgO}) \quad (110)$$

As for the actual mechanism of MgO reduction by ferrosilicon, it has been proposed (125) that the process be viewed as a metathetical reaction between MgO and SiO_2, both of which are considered to be components of the molten slag phase:

$$2MgO(\ell, \text{slag}) + Si(\ell, \text{metal}) = 2Mg(g) + SiO_2(\ell, \text{slag}) \quad (111)$$

For reaction (111) to occur the liquid metal phase should come in contact with the slag. Christini (125) considered two possible sites of contact: (a) between freshly charged liquid ferrosilicon droplets and slag near the top of the slag bath, and (b) the slag-residual ferrosilicon interface at the bottom of the furnace. He attempted to elucidate the mechanism of the reduction by comparing the calculated silicon and aluminum contents of ferrosilicon at the two possible sites of reaction, (a) and (b) above, with plant data. The calculation was based on the assumption that the aluminum and silicon of the residual ferrosilicon should be in equilibrium with Al_2O_3 and SiO_2 in the slag. Such calculations involve the use of equations (107) and (110) for which an estimation of activities and vapor pressures is required. Fortunately the quarternary system $CaO\text{-}SiO_2\text{-}Al_2O_3\text{-}MgO$ is of importance to steelmaking and has been studied extensively. Christini (125) concluded that the Magnetherm slag is a two-phase mixture exhibiting double saturation with $2CaO{\cdot}SiO_2$ and MgO, which allows good estimates for the activities to be made ($a_{MgO} = 1$, $a_{SiO_2} = 0.001$).

Regarding the magnesium pressures to be used in equations (107) and (110),

Christini (125) made the assumption that at the surface of the slag the magnesium pressure is that of the vacuum system, i.e., $P_{Mg}(surface) = P_{furnace} = 0.05$ atm., which is tantamount to assuming the instantaneous attainment of equilibrium. The pressure required for the nucleation of a magnesium droplet at the ferrosilicon-slag interface is a function of the slag depth, which increases over the course of the operation cycle and is given as P(interface) = P(furnace) + P(slag).

An assumption of a slag depth of 1.5 m was made by Christini (125), who calculated the silicon and aluminum contents of ferrosilicon at the surface to be 19.5% and 0.16%, respectively. These compare well with plant data of 20% and 0.26%, respectively. Thus, magnesium is produced at the ferrosilicon droplet-slag interface near the surface of the slag by a mechanism probably limited only by heat transfer from the heat source below. Such interpretation leads to a significant conclusion regarding the operation of the Magnetherm reduction furnace: the reduction reaction occurs mainly near the surface of the slag, and the large volume of the slag accumulated during the operation cycle plays little role in enhancing the reaction kinetics. Furthermore, from an energetic standpoint it may be beneficial to reduce slag depth. Condensation kinetics are felt to be rate limiting.

3.2.2 Reduction with aluminum

As Figure 14 shows, aluminum or aluminum alloys are much more effective as reducing agents than silicon or silicon alloys. Research on this subject has been limited due to fact that aluminum and magnesium are competitors in the marketplace. Low-grade aluminum-silicon alloys have been mentioned for possible use, but their availability and price are not stable enough to sustain a commercial magnesium process.

Nevertheless, Grjotheim et al. (132) studied the reduction of magnesium compounds with metallic aluminum by measuring the equilibrium vapor pressure of magnesium by means of a transportation method and used X-ray diffraction techniques to identify the end products of the reactions. They suggested that the reduction of pure MgO proceeds according to the reaction

$$4MgO(s) + 2Al(\ell) = MgAl_2O_4(s) + 3\,Mg(g) \qquad (112)$$

The magnesium pressure over this system is given in Table 8 and plotted in Figure 17. Much higher pressures of magnesium vapor are produced than those when silicon is the reducing agent.

Grjotheim et al. (132) also investigated the reduction of calcined dolomite (CaO·MgO) and olivine $(Mg{\cdot}Fe)_2SiO_4$, which are reduced according to the reactions

$$12CaO(s,\ dolomite) + 21MgO(s,\ dolomite) + 14Al(\ell) = 12CaO{\cdot}7Al_2O_3(s) + 21\ Mg(g) \qquad (113)$$

and

$$4MgO(s,\ olivine) + Si{\cdot}2Al(\ell,\ metal) = MgAl_2O_4(s) + Si(s) + 3Mg(g) \qquad (114)$$

A modification of aluminothermic reduction has been described (133), the so-called MC process, in which an iron aluminum alloy is produced in an electric furnace, and then in a second electric furnace dolomite is reduced by this alloy.

3.3 Other Methods of Reduction

Calcium carbide may be used to reduce either MgO (134) or $MgCl_2$ (135) at temperatures lower than the silicothermic reduction by the Pidgeon process.

The reduction of MgO proceeds according to the reaction

$$MgO(s) + CaC_2(s) = Mg(g) + CaO(s) + 2C(s) \qquad (115)$$

and reportedly (11) this process was used during World War II in the U.K. but was abandoned later due to high production costs.

The reduction of $MgCl_2$ proceeds according to the reaction

$$MgCl_2(\ell) + CaC_2(s) = Mg(g) + CaCl_2(\ell) + 2C(s) \qquad (116)$$

A process based on this reaction would require as individual steps the costly production of anhydrous magnesium chloride and the production of calcium carbide in an electric furnace; thus, it would not be able to compete successfully with the electrolytic processes.

Because both carbides and ferroalloys of highly reactive metals are produced in electric furnaces, they have been termed "canned electricity" by some authors who therefore view the viability of these reagents as thermochemical reductants for magnesium oxide with skepticism (11).

3.4 Flux Chemistry

An article on the chemistry of magnesium production would not be complete without at least a brief reference to the role of flux chemistry in the

production of high purity magnesium metal and magnesium alloys of specified composition.

The term 'flux' is used in the context of a chemical reagent (which may be a multicomponent solution) capable of acting in one or more of the following ways: to protect the molten magnesium from contamination by reaction with the atmosphere, to refine contaminants out of the molten magnesium, or to help introduce alloying elements in controlled quantities into the molten magnesium.

Fluxes for protection establish a physical barrier to mass transport of atmospheric species to the molten metal surface beneath. The flux in this case can be either a liquid, such as a chloride-based melt, or a gas, such as air containing SF_6 and CO_2 (136).

For the refining of magnesium the impure molten metal is covered by a liquid phase flux with which it is immiscible. Through metathetical reactions contaminants are removed. For example, Magnetherm product has reportedly (137) been refined by a carnallite-type flux containing 55% KCl. The calcium and sodium concentrations are reduced to acceptable levels according to the reaction

$$2(K_2MgCl_4) + \underline{Ca} + \underline{Na} = (CaCl_2) + 2(NaCl) + 4(KCl) + 2\underline{Mg} \qquad (117)$$

where the underline denotes that the species is dissolved in the metal phase and the parentheses denote that the species is dissolved in the molten flux phase. Molten magnesium also contains solid particles, mainly metal oxides. The chloride flux then serves as a sink for the removal of these particles which otherwise become nonmetallic inclusions when the metal solidifies.

Alloying is done in much the same manner as refining, namely by metathetical reactions with a molten flux in contact with magnesium metal.

4. FUTURE OUTLOOK

It is somewhat ironic that the least dense structural metal, magnesium, which can reduce energy consumption when used as a material for vehicular construction, is one of the most energy-intensive metals to produce with presently available technologies. Thus efforts to reduce the cost of production must address the energy requirements of extraction and bring them closer to the theoretical minima. An understanding of the scientific principles of the relevant chemistry and electrochemistry serves to specify these theoretical limitations and to guide research and development in this regard.

In electrolytic processes, cell feed preparation is energy-intensive (18). New chemistries for energy-efficient dehydration of $MgCl_2$ may be found through the use of organic media. This requires the involvement of scientific personnel from outside the field of classical chemical metallurgy. A more remote possibility is the replacement of $MgCl_2$ as the cell feed in favor of a different magnesium-bearing compound that both has a lower decomposition potential and requires less energy to prepare (45).

As for the electrolysis operation itself, improvements in energy efficiency will accrue from decreasing the cell voltage. This can be accomplished through changes in cell design and the use and development of new materials. New cell designs must reduce internal cell resistance. Improved diaphragmless cells and multipolar electrode configurations are two possibilities that in the past have not been fully exploited due to materials limitations. However, the advent of a new generation of high performance materials now offers a new opportunity for success. For example, TiB_2, which has been extensively tested by the aluminum industry as a candidate cathode material in Hall-Heroult cells, may be extremely useful as an electrode material in advanced magnesium cell designs.

Control of the flow patterns of the various fluids present, namely molten electrolyte, molten magnesium, and anode gases, is also very important in decreasing cell resistance. With a better understanding of the fluid mechanics of such multiphase flows, their circulation can be optimized. Related to this is the question of the use of LiCl-based supporting electrolytes to facilitate separation of cell products. Finally, no discussion of energy efficiency would be complete without mention of the need for developing on-line process control. Perhaps high-speed electrochemical and spectroscopic techniques have an important role to play in sensing and monitoring cell performance.

In the non-electrolytic processes, improvements in energy efficiency are somewhat restricted by the fact that these are batch operations. While continuous operations offer economy by control of throughput, batch operations through tighter control of process chemistry have the potential to produce metal of very high purity. This coupled with further developments in on-line process control could pave the way for a highly automated process offering product reliability. Internally heated reactors, such as Magnetherm, have the greatest potential for such automation.

Greater utilization of magnesium will not be achieved through process innovation alone. There are other obstacles.

Rather than a structural material, magnesium today is primarily a chemical

reagent: an alloying addition to aluminum (which is the structural material in this case), a chemical reductant for sulfur in steel, a chemical reactant in the synthesis of Grignard reagents, etc. If magnesium is to realize its full potential it must become more fully exploited in structural applications where it competes with other materials, both metallic, principally aluminum, and nonmetallic, namely plastics. Magnesium has had limited success in penetrating markets traditionally held by its competitors. Two developments can improve this situation. First, new magnesium-based alloys must be developed with unique properties that place magnesium ahead of the competition. Two examples are ultralight alloys and ultrastiff alloys. Secondly, the corrosion resistance of existing magnesium-based alloys that otherwise compete favorably in today's structural markets must be improved. New metal processing technologies such as rapid solidification may make major contributions in both areas.

As our understanding of materials evolves from viewing them as commodities to viewing them as "bundles of properties", the strong attributes of magnesium will become the basis for its almost certain greater utilization.

ACKNOWLEDGEMENTS

The authors wish to acknowledge the following individuals, organizations and agencies:

for their careful review of the manuscript and for their helpful suggestions, Mr. Cliff B. Wilson, Dow Chemical Company; Drs. Roy A. Christini and Kenneth A. Bowman, Alcoa; Dr. R. Neelameggham, AMAX Magnesium Corp., Mr. John C. Priscu, Chem-Pro Consultants, Inc.; and Mr. Alfred H. Wheeler, MPLC, North American Magnesium, Inc.,

for conducting plant tours, Dr. Ken Claus, Dow Chemical Company, and Drs. Michel Demange and Christian Payn, Pechiney Electrometallurgie,

for partial financial support, the U.S. Department of Energy, Office of Industrial Programs.

REFERENCES

1. L.F. Lockwood, G. Ansel and P.O. Haddad, in "Kirk-Othmer Encyclopedia of Chemical Technology," 3rd Ed., 14, Wiley, New York, 1981, pp. 570-615.
2. Kh.L. Strelets, "Electrolytic Production of Magnesium," translated by J. Schmorak, Keter, Jerusalem, 1977. also available as TT 76-50003, U.S. Dept. Commerce, NTIS, Springfield VA.
3. R.D. Goodenough and V.A. Stenger, in J.C. Bailar, Jr., H.J. Emeleus, Sir R. Nyholm, and A.F. Trotman-Dickenson (Eds.), "Comprehensive Inorganic Chemistry," 1, Pergamon, Oxford, 1973, pp. 591-663.
4. "Standard Specification for Magnesium Ingot and Stick for Remelting," ASTM Designation 392-80 (Reapproved 1985), Annual Book of ASTM Standards, Volume 02.02, ASTM, Philadelphia PA, 1986, pp. 80-81.
5. A.H. Schultz, R. Neelameggham, J.C. Agarwal and E.W. Hammersley, in H.O. Bohner (Ed.), "Light Metals 1985," TMS/AIME, Warrendale PA, 1985, p. 1475.
6. W.J. Kroll, Rev. Metall., 48 (1951) 929.
7. A. Beck, "Technology of Magnesium and its Alloys," Hughes, London, 1940.
8. Magnesium, American Society for Metals, Cleveland OH, 1946.
9. G.V. Raynor, "The Physical Metallurgy of Magnesium and its Alloys," Pergamon, London, 1959.
10. C.S. Roberts, "Magnesium and its Alloys," Wiley, New York, 1960.
11. E.F. Emley, "Principles of Magnesium Technology," Pergamon, London, 1966.
12. D. Gilroy, in A.T. Kuhn (Ed.), "Industrial Electrochemical Processes," Elsevier, Amsterdam, 1971, pp. 175-217.
13. N. Jarrett, in J.K. Tien and J.F. Elliott (Eds.), "Metallurgical Treatises," TMS/AIME, Warrendale PA, 1981, pp. 159-169.
14. D. Pletcher, "Industrial Electrochemistry," Chapman & Hall, London, 1982.
15. K.C. Dean, D.A. Elkins and S.J. Hussey, "An Economic and Technical Evaluation of Magnesium Production Methods. 1. Metallothermic," U.S. Bur. of Mines, R.I. 6656, 1965.
16. D.A. Elkins, P.L. Placek and K.C. Dean, "An Economic and Technical Evaluation of Magnesium Production Methods. 2. Carbothermic," U.S. Bur. of Mines, R.I. 6946, 1967.
17. D.A. Elkins, K.C. Dean and J.B. Rosenbaum, "Economic Aspects of Magnesium Production," Proceedings of Extractive Metallurgy Division Symposium on Electrometallurgy, AIME, Cleveland OH, Dec. 1968, 173-184.
18. G.B. Kenney, D.R. Sadoway and M.C. Flemings, in "Proceedings of the 37th Annual World Conference on Magnesium," International Magnesium Association, Dayton, OH, 1980, pp. 14-18.
19. "Trends in Usage of Magnesium," Publication NMAB-322, National Academy of Sciences, Washington, D.C., 1975.
20. "The Economics of Magnesium," 2nd Ed., Roskill Information Services, Ltd., London, 1978.
21. M.W. Chase, J.L. Curnutt, R.A. McDonald and A.N. Syverud, JANAF Thermochemical Tables, 1978 Supplement, J. Phys. Chem. Ref. Data, 7 (3) (1978) 793.
22. N. Høy-Petersen, Light Metal Age, 35 (1977) 9.
23. J.W. Mellor, "A Comprehensive Treatise on Inorganic and Theoretical Chemistry," Vol. 4, Longmans, Green and Co., New York, 1940, pp. 249-397.

24. Gmelins Handbuch der Anorganischen Chemie, Vol. 27, Verlag Chemie, Berlin, 1939, pp. 114-122.
25. K.K. Kelley, "Energy Requirements and Equilibria in the Dehydration, Hydrolysis and Decomposition of Magnesium Chlorides," U.S. Bur. of Mines, Technical Paper 676, 1945.
26. K.K. Kelley, "Contributions to the Data on Theoretical Metallurgy," U.S. Bur. of Mines, Bulletin 584, 1960.
27. S. Fougner, in H. Forberg (Ed.), "Light Metals, 1974," Vol. 2, TMS/AIME, New York, 1974, pp. 515-533.
28. E.W. Barlow, S.C. Johnson and A. Sadan, in C.J. McMinn (Ed.), "Light Metals 1980," TMS/AIME, Warrendale PA, 1979, pp. 913-927.
29. H.-H. Emons, R. Naumann, T. Pohl and A. Voigt, J. Thermal Anal., 29 (1984) 571.
30. D. Petzold and R. Naumann, J. Thermal Anal., 19 (1980) 25.
31. W.K. Behl and H.C. Gaur, J. Sci. Instr. Res., 20B (1961) 231.
32. M. Nakayasu, Y. Sugukawa, W. Kobayashi and K. Usui, in "First International Symposium on Molten Salt Chemistry and Technology," Kyoto, Japan, 1983, pp. 119-122.
33. R.J. Allain, in C.J. McMinn (Ed.), "Light Metals 1980," TMS/AIME, Warrendale PA, 1979, pp. 929-936.
34. S.-Y. Yoon, J.H. Flint, G.J. Kipouros and D.R. Sadoway, in R.G. Bautista and R.J. Wesely (Eds.), "Energy Reduction Techniques in Metal Electrochemical Processes," TMS/AIME, Warrendale PA, 1985, pp. 479-491.
35. C.E.E. Shackleton, E.A.B. Shackleton, A.J. Wickens and J.H.W. Turner, inventors, Mineral Process Licensing Corp. BV, assignee, U.S. patent no. 4,269,816, May 26, 1981.
36. D.E. Neil, H.M. Clark and R.H. Wiswall, Jr., J. Chem. Eng. Data, 10 (1965) 21.
37. S.N. Flengas, in C.H. Hampel (Ed.), "The Encyclopedia of Electrochemistry," Kreiger, Huntington NY, 1972, pp. 644-649.
38. Yu.K. Delimarsky and B.F. Markov, "Electrochemistry of Fused Salts," translated by R.E. Wood, Sigma Press, Washington, D.C., 1961.
39. G.J. Janz, C.B. Allen, N.P. Bansal, R.M. Murphy and R.P.T. Tomkins, Physical Properties Data Compilations Relevant to Energy Storage. II. Molten Salts: Data on Single and Multicomponent Salt Systems, NSRDS-NBS-61, Part II, 1979.
40. E.A. Brandes (Ed.), "Smithells Metals Reference Book," 6th edition, Butterworths, London, 1983.
41. A.A. Maurits, J. Appl. Chem. USSR, 44 (1971) 1671.
42. N. Høy-Petersen, J. Metals, 21 (1969) 43.
43. R.D. Holliday and P. McIntosh, J. Electrochem. Soc., 120 (1973) 858.
44. V.V. Stender, P.B. Zivotinsky and M.M. Stroganoff, Trans. Electrochem. Soc., 65 (1934) 189.
45. R. Neelameggham and J.C. Priscu, in R.G. Bautista and R. Wesely (Eds.), "Energy Reduction Techniques in Metal Electrochemical Processes," TMS/AIME, Warrendale PA, 1985, pp. 445-452.
46. P. Kozakevitch, in "Surface Phenomena of Metals," Soc. Chem. Ind., London, Monograph No. 28, 1968, pp. 223-245.
47. G.M. Rao, J. Appl. Electrochem., 16 (1986) 775.
48. F.J. Krenzke, in C.A. Hampel (Ed.), "The Encyclopedia of Electrochemistry," Krieger, Huntington NY, 1972, pp. 783-787.
49. C. Sandonnini, Atti Accad. Naz-Lincei, Rend., Classe Sci. Fiz., Mat. Nat., 22 (1931) 631.
50. W. Klemm and P. Weiss, Z. anorg. allgem. chem., 245 (1940) 281.
51. K. Grjotheim, J.L. Holm and M. Roetnes, Acta Chem. Scand., 26 (1972) 3802.

52. A.I. Ivanov, Sb. Stat. Obshch. Khim., Akad. Nauk SSSR, 1 (1953) 754.
53. B.F. Markov and I.D. Panchenko, Zh. Obshch. Khim., 25 (1955) 2039.
54. B.F. Markov and I.D. Panchenko, Zh. Obshch. Khim., 25 (1955) 2042.
55. T. Førland, Freezing Point Depression and its Structural Interpretation, Office of Naval Research Technical Report No. 63, 1955.
56. H. Flood and S. Urnes, Z. Elektrochem., 59 (1955) 834.
57. O.J. Kleppa and F.G. McCarty, J. Phys. Chem., 70 (1966) 1249.
58. H.T. Davis, J. Chem. Phys., 41 (1964) 2761.
59. B.F. Markov, Yu.K. Delimarsky and I.D. Panchenko, Zh. Fiz. Khim., 29 (1955) 51.
60. T. Østvold, Acta Chem. Scand., 23 (1969) 688.
61. H. Ikeuchi and C. Krohn, Acta Chem. Scand., 23 (1969) 2230.
62. A.D. Pelton and W.T. Thompson, Can. J. Chem., 48 (1970) 1585.
63. J. Braunstein, J. Chem. Phys., 49 (1968) 3508.
64. K. Balasubrahmanyam, J. Chem. Phys., 44 (1966) 3270.
65. V.A. Maroni and E.J. Cairns, in G. Mamantov (Ed.), "Molten Salts," Marcel Dekker, New York, 1969, pp. 231-289.
66. V.A. Maroni, E.J. Hathaway and E.J. Cairns, J. Phys. Chem., 75 (1971) 155.
67. V.A. Maroni, J. Chem. Phys., 55 (1971) 4789.
68. R.J. Capwell, Chem. Phys. Lett., 12 (1972) 443.
69. M.H. Brooker, J. Chem. Phys., 63 (1975) 3054.
70. C.H. Huang and M.H. Brooker, Chem. Phys. Lett., 43 (1976) 180.
71. M.H. Brooker and C.H. Huang, Can. J. Chem., 58 (1980) 168.
72. C.S. Gibbons, V.C. Reinsborough and W.A. Whitla, Can. J. Chem., 53 (1975) 114.
73. M.M. Laursen and J.H. von Barner, J. Inorg. Nucl. Chem., 41 (1979) 185.
74. S.-Y. Yoon, J.H. Flint, G.J. Kipouros and D.R. Sadoway, in R.E. Miller (Ed.), "Light Metals 1986," TMS/AIME, Warrendale PA, 1986, pp. 1009-1012.
75. S.-Y. Yoon and D.R. Sadoway, in R.D. Zabreznik (Ed.), "Light Metals 1987," TMS/AIME, Warrendale PA, 1987, pp. 851-859.
76. R.M. Hunter, Trans. Electrochem. Soc., 86 (1945) 21.
77. T.R. Beck and R.T. Ruggeri, in H. Gerischer and C.W. Tobias (Eds.), "Advances in Electrochemistry and Electrochemical Engineering," Vol. 12, Wiley, New York, 1981, pp. 263-354.
78. E. Aarebrot, R.E. Andresen, T. Østvold and H.A. Øye, in K.B. Higbie (Ed.), "Light Metals 1977," Vol. 1, TMS/AIME, New York, 1977, pp. 491-512.
79. A. Anundskas, K. Grjotheim, A.H. Schultz, H. Svendsen and H.A. Øye, Metall (Berlin), 25 (1975) 493.
80. E.A. Ukshe, G.V. Polyanova and G.A. Medvetskaya, J. Appl. Chem. USSR, 33 (1960) 2246.
81. T. Østvold and H.A. Øye, in C.J. McMinn (Ed.), "Light Metals 1980," TMS/AIME, Warrendale PA, 1979, pp. 937-947.
82. R. Tunold, in C.J. McMinn (Ed.), "Light Metals 1980," TMS/AIME, Warrendale PA, 1979, pp. 949-957.
83. A. Komura, H. Imanaga and N. Watanabe, Denki Kagaku, 40 (1972) 762.
84. P.A. Donskikh, Elektrokhimiya, 21 (1985) 878.
85. G.M. Rao, J. Appl. Electrochem., 16 (1986) 626.
86. S.A. Pushkareva, and E.A. Ukshe, Dokl. Akad. Nauk SSSR, 124 (1959) 370.
87. E.A. Ukshe and S.I. Stepanov, Zh. Fiz. Khim., 34 (1960) 265.
88. F. Oettel, Z. Elektrochem., 2 (1895) 394.
89. Kh.Kh. Sabirov, N.V. Bondarenko and M. Gurinovich, Zh. Prikl. Khim., 51 (1978) 1572.

90. D.R. Sadoway, Transport Phenomena in Improved Electrochemical Cell Designs for the Production of Magnesium, Final Report, U.S. Dept. of Energy, Report No. DOE/CE/90033-6, Sept. 1, 1983.
91. N.G. Bukun and E.A. Ukshe, Dokl. Akad. Nauk SSSR, 128 (1959) 121.
92. N.G. Bukun and E.A. Ukshe, Russ. J. Inorg. Chem., 6 (1961) 465.
93. J.D. Van Norman and J.J. Egan, J. Phys. Chem., 67 (1963) 2460.
94. M. Krumpelt, J. Fischer and I. Johnson, J. Phys. Chem., 72 (1968) 506.
95. R. Minami, T. Nakajima and N. Watanabe, Nippon Kagaku Kaishi, 11 (1975) 1895.
96. A. Komura, H. Imanaga and N. Watanabe, Denki Kagaku, 41 (1973) 281.
97. E. Aarebrot, R.E. Andresen, T. Østvold and H.A. Øye, Metall (Berlin), 32 (1978) 41.
98. J. Wypartowicz, T. Østvold and H.A. Øye, Electrochim. Acta, 25 (1980) 151.
99. H.J.T. Ellingham, J. Soc. Chem. Ind. (London), 63 (1944) 125.
100. T. Rosenqvist, "Thermochemical Data for Metallurgists," Tapir Forlag, Norway, 1970.
101. H.A. Glassner, The Thermochemical Properties of the Oxides, Fluorides and Chlorides to 2500°K, Argonne National Laboratory, ANL-5750, 1965.
102. T.B. Reed, "Free Energy of Formation of Binary Compounds," MIT Press, Cambridge MA, 1971.
103. T.A. Dungan, Trans. AIME, 159 (1944) 308.
104. F.J. Hansgirg, Iron Age, 152 (21) (1943) 56; 152 (22) (1943) 52.
105. L.M. Pidgeon, Trans. Can. Inst. Min. Met., 47 (1944) 17.
106. L.M. Pidgeon and W.A. Alexander, Trans. AIME, 159 (1944) 315.
107. L.M. Pidgeon, Trans. Can. Inst. Min. Met., 49 (1946) 621.
108. W.B. Humes, Trans. AIME, 159 (1944) 353.
109. A. Mayer, Trans. AIME, 159 (1944) 363.
110. W.M. Peirce, R.K. Waring, L.D. Fetterolf and G. Mahler, Trans. AIME, 159 (1944) 377.
111. E. Schrier, Chem. Eng., 59 (4) (1952) 148.
112. A. Froats, in C.J. McMinn (Ed.), "Light Metals 1980," TMS/AIME, Warrendale PA, 1979, pp. 969-979.
113. E.G. DeCoriolis, Trans. AIME, 182 (1949) 93.
114. B. Ellingsaeter and T. Rosenqvist, J. Metals, 8 (1956) 1111.
115. A. Schneider and E. Hesse, Z. Elektrochem., 46 (1940) 279.
116. W.J. Kroll, Light Metals, 7 (1944) 465.
117. L.M. Pidgeon and J.A. King, Disc. Faraday Soc., 4 (1948) 197.
118. A. Schneider, Z. Metallk., 41 (1950) 205.
119. O. Kubaschewski, E.L. Evans and C.B. Alcock, "Metallurgical Thermochemistry," 4th edition, Pergamon, London, 1967, pp. 238-240.
120. A. Schneider, J.F. Cordes, H. Kribbe and H. Runge, Erzbergbau Metallhuttenw., 12 (1959) 103-111, 164-172, 224-226.
121. J.M. Toguri and L.M. Pidgeon, Can. J. Chem., 39 (1961) 540.
122. J.M. Toguri and L.M. Pidgeon, Can. J. Chem., 40 (1962) 1769.
123. J.R. Wynnyckyj and L.M. Pidgeon, Metall. Trans., 2 (1971) 975.
124. J.R. Wynnyckyj and L.M. Pidgeon, Metall. Trans., 2 (1971) 979.
125. R.A. Christini, in C.J. McMinn (Ed.), "Light Metals 1980," TMS/AIME, Warrendale PA, 1979, pp. 981-995.
126. C. Faure and J. Marchal, J. Metals, 16 (1964) 721.
127. F. Trocme, in T.G. Edgeworth (Ed.), "Light Metals 1971," TMS/AIME, Warrendale PA, 1971, pp. 669-677.
128. M.P. Lugagne, Erzmetall., 31 (1978) 310.
129. J.M. Logerot and A.M. Mena, Extractive Metallurgy: Latest Developments of the Magnetherm Process, TMS Paper Selection, CM-80-74, TMS/AIME, Warrendale PA, 29 pp.

130. R.A. Christini, R. Rolles, K.A. Bowman and M.D. Ballain, U.S. patent no. 4,478,637, Oct. 23, 1984.
131. K.A. Bowman, R.A. Christini and M.D. Ballain, U.S. patent no. 4,498,927, Feb. 12, 1985.
132. K. Grjotheim, O. Herstad and J.M. Toguri, Trans. Can. Inst. Min. Met., 65 (1962) 221.
133. G.N. Kirsebom, Light Metals and Metal Industry, 27 (Feb.) (1964) 44.
134. G.L. Miller, Vacuum, 2 (1952) 19.
135. L.R. Michels, B. Cartwright and S.F. Ravitz, U.S. Bur. of Mines, R.I. 4059, 1947.
136. S.L. Couling and T.E. Leontis, in C.J. McMinn (Ed.), "Light Metals 1980," TMS/AIME, Warrendale PA, 1979, pp. 997-1009.
137. K.A. Bowman, in R.E. Miller (Ed.), "Light Metals 1986," TMS/AIME, Warrendale PA, 1986, pp. 1033-1038.